10-2008

Neutrino-Nucleus Reaction Cross Sections for Light Element Systhesis in Supernova Explosions

Takashi Yoshida
National Astronomical Observatory of Japan - Osawa, Mitakga, Tokyo, takashi.yoshida@nao.ac.jp

Toshio Suzuki
Department of Physics, College of Humanities and Science, Nihon University & Center for Nuclear Study, University of Tokyo

Satoshi Chiba
Advanced Science Research Center, Japan Atomic Energy Agency

Toshitaka Kajino
National Astronomical Observatory, and The Graduate University forAdvanced Studies & Department of Astronomy, Graduate School of Science, University ofTokyo

Hidekazu Yokomakura
Department of Physics, Graduate School of Science, Nagoya University,

See next page for additional authors

The Astrophysical Journal, 686:448–466, 2008 October 10

NEUTRINO-NUCLEUS REACTION CROSS SECTIONS FOR LIGHT ELEMENT SYNTHESIS IN SUPERNOVA EXPLOSIONS

Takashi Yoshida,[1] Toshio Suzuki,[2,3] Satoshi Chiba,[4] Toshitaka Kajino,[5,6] Hidekazu Yokomakura,[7] Keiichi Kimura,[7] Akira Takamura,[8] and Dieter H. Hartmann[9]

Received 2008 January 30; accepted 2008 June 18

ABSTRACT

The neutrino-nucleus reaction cross sections of ^{4}He and ^{12}C are evaluated using new shell model Hamiltonians. Branching ratios of various decay channels are calculated to evaluate the yields of Li, Be, and B produced through the ν-process in supernova explosions. The new cross sections enhance the yields of ^{7}Li and ^{11}B produced during the supernova explosion of a 16.2 $M_\odot$ star model compared to the case using the conventional cross sections by about 10%. On the other hand, the yield of ^{10}B decreases by a factor of 2. The yields of ^{6}Li, ^{9}Be, and the radioactive nucleus ^{10}Be are found at a level of $\sim 10^{-11}$ $M_\odot$. The temperature of $\nu_{\mu,\tau}$- and $\bar{\nu}_{\mu,\tau}$-neutrinos inferred from the supernova contribution of ^{11}B in Galactic chemical evolution models is constrained to the 4.3–6.5 MeV range. The increase in the ^{7}Li and ^{11}B yields due to neutrino oscillations is demonstrated with the new cross sections.

Subject headings: neutrinos — nuclear reactions, nucleosynthesis, abundances — supernovae: general

Online material: color figures, machine-readable tables

1. INTRODUCTION

Supernova (SN) explosions constitute one of several production sites of the relatively rare light elements Li, Be, and B. In SN environments these elements are produced through neutrino-nucleus reactions (the ν-process; Domogatsky et al. 1978; Woosley et al. 1990). Neutrinos of all flavors are emitted in large numbers from a proto–neutron star, created during core-collapse of massive stars and the subsequent supernova explosion. Among the light elements, ^{7}Li and ^{11}B are abundantly produced through the ν-process (Woosley et al. 1990; Yoshida et al. 2004, 2005a; Heger et al. 2005). Production of these light element isotopes in core-collapse supernovae (ccSNe) can contribute significantly to the increase in their abundances during Galactic chemical evolution (GCE; Fields et al. 2000; Ramaty et al. 2000a, 2000b).

Cross sections for neutrino-nucleus interactions are some of the most important data required to reliably estimate the ^{7}Li and ^{11}B yields in supernovae. The ν-process cross sections have been evaluated for a wide range of nuclear species in Woosley et al. (1990). The data are tabulated in Hoffman & Woosley (1992, hereafter referred to as HW92).[10] Since the evaluation by HW92, further development of shell model calculations now enable us to more accurately evaluate these essential cross sections.

The ν-process cross sections are often presented as a function of neutrino temperature, based on averaging energy-dependent cross sections over a Fermi-Dirac distribution of given temperature and chemical potential (for simplicity often assumed to be zero). However, it is more appropriate to consider the energy dependence as the primary information, as studies of SN neutrino transport show that their spectra do not exactly follow Fermi-Dirac distributions with zero chemical potential (e.g., Keil et al. 2003). Furthermore, when considering neutrino oscillations in SNe, the spectra are nonthermal after the neutrino flavors change, even if the Fermi-Dirac distribution approximates the spectra at the neutrino sphere reasonably well (e.g., Dighe & Smirnov 2000; Takahashi et al. 2001).

The main purpose of this study is the reevaluation of neutrino-nucleus reaction cross sections for ^{12}C and ^{4}He using new shell-model Hamiltonians. We evaluate the branching ratios of many decay channels for light element species. Then, we evaluate the yields of the light elements, ^{6}Li, ^{7}Li, ^{9}Be, ^{10}Be, ^{10}B, and ^{11}B, and discuss their production processes. We reestimate the allowed range of the neutrino temperatures derived from constraints on the SN contribution of ^{11}B in GCE models (following Yoshida et al. 2005a). We also investigate the dependence of the neutrino oscillation parameters, i.e., mass hierarchy and the mixing angle θ_{13}, on the ^{7}Li and ^{11}B yields using the new cross sections.

The paper is organized as follows. In § 2, new cross sections for neutrino-^{12}C reactions are derived using the SFO and PSDMK2 Hamiltonians. New cross sections for neutrino-^{4}He reactions are evaluated using the WBP and SPSDMK Hamiltonians, as also shown in this section. The temperature dependence of the cross sections is discussed. The supernova explosion model and supernova neutrino models employed are introduced and explained in detail in § 3. The nuclear reaction network used in this study is presented briefly. Light-element production mechanisms are discussed in § 4. The yields obtained using the new cross sections and the differences from those obtained with old cross sections are shown. The dependence of the light-element yields on neutrino chemical potential is also discussed. The dependence of the

[1] National Astronomical Observatory of Japan, 2-21-1 Osawa, Mitaka, Tokyo 181-8588, Japan; takashi.yoshida@nao.ac.jp.
[2] Department of Physics, College of Humanities and Science, Nihon University, Sakurajosui 3-25-40, Setagaya-ku, Tokyo 156-8550, Japan.
[3] Center for Nuclear Study, University of Tokyo, Hirosawa, Wako-shi, Saitama 351-0198, Japan.
[4] Advanced Science Research Center, Japan Atomic Energy Agency, 2-4 Shirakata-shirane, Tokai, Ibaraki 319-1195, Japan.
[5] National Astronomical Observatory, and The Graduate University for Advanced Studies, 2-21-1 Osawa, Mitaka, Tokyo 181-8588, Japan.
[6] Department of Astronomy, Graduate School of Science, University of Tokyo, 7-3-1 Hongo, Bunkyo-ku, Tokyo 113-0033, Japan.
[7] Department of Physics, Graduate School of Science, Nagoya University, Furo-cho, Chikusa-ku, Nagoya, Aichi 464-8602, Japan.
[8] Department of Mathematics, Toyota National College of Technology, Eisei-cho 2-1, Toyota, Aichi 471-8525, Japan.
[9] Department of Physics and Astronomy, Clemson University, Clemson, SC 29634.
[10] See http://www-phys.llnl.gov/Research/RRSN/nu_csbr/neu_rate.html.

yields of ^{7}Li and ^{11}B on the neutrino oscillation parameters, mass hierarchy, and the mixing angle θ_{13} is shown in § 5. The dependence of neutrino oscillation parameters on the ^{7}Li/^{11}B ratio, the elemental abundance ratios of the light elements, is considered, and the possibility of constraining mass hierarchies and the mixing angle θ_{13} is evaluated. Other effects on flavor exchange of neutrinos in supernovae are discussed in § 6, and our conclusions are finally presented in § 7.

2. NEUTRINO-NUCLEUS REACTION CROSS SECTIONS OF ^{4}He AND ^{12}C

New neutrino-induced reaction cross sections on ^{12}C have been obtained by shell model calculations with the SFO Hamiltonian (Suzuki et al. 2006, hereafter SC06). The SFO Hamiltonian describes spin properties of p-shell nuclei, such as Gamow-Teller (GT) transitions, better than conventional shell-model Hamiltonians, such as PSDMK2 (Millener & Kurath 1975; Brown et al. 1986). Systematic improvements in the agreement between calculated and observed magnetic moments of p-shell nuclei supports the use of the SFO Hamiltonian (Suzuki et al. 2003a), which takes into account the important roles of spin-isospin interactions, in particular tensor interaction, and is found to lead to proper shell evolution (Otsuka et al. 2005; Suzuki et al. 2006).

While a slight modification of the axial-vector coupling constant, $g_A^{\rm eff}/g_A = 0.95$, is enough to reproduce the GT transition in ^{12}C, a large quenching of the coupling constant, $g_A^{\rm eff}/g_A = 0.7$, was taken for other multipoles to reproduce the inclusive charged-current reaction cross sections induced by the DAR neutrinos (Suzuki et al. 2006). This is consistent with the electron scattering data, where considerable quenching of the spin g-factor, $g_s^{\rm eff}/g_s = 0.6$–0.7, explains the M2 form factor in ^{12}C (2^-, $T = 1$, 19.40 MeV) at low momentum transfer (Drake et al. 1968; Yamaguchi et al. 1971; Gaarde et al. 1984). The final state interaction is included by multiplying the relativistic Fermi function for the charged-current reactions.

Although large quenching of $g_A^{\rm eff}/g_A = 0.7$ was adopted for all multipoles other than the GT transitions in Suzuki et al. (2006), electron scattering data indicate a smaller quenching of the spin g-factor for 1^- states, i.e., $g_s^{\rm eff}/g_s \approx 0.9$ (Drake et al. 1968; Yamaguchi et al. 1971). Photoreaction cross section data indicate that the electric dipole transition strength is quenched by about 30% below $E_x = 30$ MeV, and a large fraction of the strength is pushed up to higher energy (Ahrens et al. 1975; Pywell et al. 1985; McLean et al. 1991; Suzuki et al. 2003b). We therefore adopt separate quenching factors for g_A: $g_A^{\rm eff}/g_A = 0.95$, 0.7, and 0.9 for the GT (1^+), 2^- spin dipole, and other multipoles, respectively. The Coulomb dipole form factor is also reduced by 30%. As the dominant contributions come from the GT and the 2^- spin-dipole transitions, the inclusive charged-current reaction cross section in ^{12}C remains to be explained by the modified quenching factors. Effects of the change of the contributions from other multipoles are insignificant. The shell-model configuration space assumed here is the same as in Suzuki et al. (2006), but multiple polarities up to $J = 4$ are included, instead of just $J = 3$.

To enable comparisons, the cross sections for ^{12}C are obtained for the conventional PSDMK2 Hamiltonian in the same way, i.e., with $g_A^{\rm eff}/g_A = 1.0$, 0.75, and 0.9 for the GT, 2^- spin-dipole, and other multipoles, respectively, and with the Coulomb dipole form factor reduced by 30%.

Neutrino-induced reaction cross sections on ^{4}He are obtained by shell-model calculations with the WBP (Warbutron & Brown 1992) and SPSDMK (Millener & Kurath 1975; Brown et al. 1986) Hamiltonians, with the bare g_A (Suzuki et al. 2006). The $0s$–$0p$–$1s0d$–$1p0f$ and $0s$–$0p$–$1s0d$ configurations are taken for the shell-model space for the WBP and SPSDMK cases, respectively, and ^{4}He is not treated as a closed core. The axial-vector coupling constant is therefore taken to be the bare value, g_A. The shell-model configuration space is extended up to 4 (5)$\hbar\omega$ excitations for positive (negative) parity transitions, instead of just up to 2 (3)$\hbar\omega$ excitations.

Branching ratios for γ transitions and proton (p), neutron (n), and α knock-out channels have been obtained from Hauser-Feshbach theory for ^{12}C (Suzuki et al. 2006). However, we extend the Hauser-Feshbach calculations by including knock-out of a deuteron (d), ^{3}He and ^{3}H, as well as multiparticle knock-out channels. All possible particle knock-out and γ transitions are included until the transitions end up with a residual nucleus with mass number $A = 6$–12. For ^{4}He, p, n, and d, knock-out channels are taken into account. Here, Hauser-Feshbach calculations are carried out for each Hamiltonian, consistently with the respective energy spectrum. We allowed α decay (1) after γ transition from isospin $T = 1$ states in ^{12}C to $T = 0$ states, or (2) directly from $T = 1$ states in ^{12}C to $T = 1$ states in ^{8}Be. We also assumed 1% isospin nonconservation in γ transitions, as the experimental data for ^{12}C indicate such a possibility.

Calculated reaction cross sections for various channels are shown in Figure 1 for ^{4}He and in Figures 2 and 3 for ^{12}C. For neutral current reactions, the average of (ν, ν') and $(\bar{\nu}, \bar{\nu}')$ reactions are shown. Nuclei produced, including those knocked out, which cannot decay further by particle emissions, are denoted in the figures.

Neutral-current and charged-current reaction cross sections on ^{4}He, ^{4}He$(\nu, \nu' p)^3$H, ^{4}He$(\nu, \nu' n)^3$He, ^{4}He$(\nu, \nu' d)^2$H, ^{4}He$(\nu, \nu' nnp)^1$H, ^{4}He$(\nu_e, e^- p)^3$He, ^{4}He$(\nu_e, e^- pp)^2$H, ^{4}He$(\bar{\nu}_e, e^+ n)^3$H, and ^{4}He$(\bar{\nu}_e, e^+ nn)^2$H, induced by supernova neutrinos with temperature T_ν, are shown in Figure 1. For these averaged cross sections, the neutrino energy spectra are assumed to be Fermi-Dirac distributions with zero chemical potential, to enable comparisons with our earlier studies. Results for the two shell-model Hamiltonians, WBP and SPSDMK, are shown. Results for ^{12}C obtained with the SFO and the PSDMK2 Hamiltonians are shown in Figures 2 and 3, respectively. We note that the decomposition cross section of ^{12}C, $\sigma_{^{12}{\rm C},\nu}$, has the following relation to the production cross section, $\sigma_{^{12}{\rm C},\nu}(Z_i, A_i)$, of species i, of which charge number and mass number are Z_i and A_i, respectively:

$$\sigma_{^{12}{\rm C},\nu} = \sum_i \frac{A_i}{12} \sigma_{^{12}{\rm C},\nu}(Z_i, A_i). \quad (1)$$

For use with nonthermal neutrino spectra, cross section values for ^{4}He as a function of the neutrino energy for the WBP and SPSDMK Hamiltonians are provided in Tables 1 and 2. The neutrino-induced reaction cross sections of ^{12}C for neutral-current reactions, charged-current reactions of ν_e, and those of $\bar{\nu}_e$ with the SFO and PSDMK2 Hamiltonians are listed in Tables 3, 4, and 5 (SFO) and 6, 7, and 8 (PSDMK2).

For ^{4}He, the neutral current reaction cross sections obtained with the WBP Hamiltonian are rather close to those obtained with a microscopic ab initio calculation using AV8' interaction (Gazit & Barnea 2004), although the dependence on T_ν is more moderate for WBP. We thus take the cross sections obtained by WBP and SFO as a "standard set" for the evaluation of the production yields of light elements during supernova explosions.

We now briefly explain important neutrino-nucleus reactions on ^{12}C, relevant for producing light elements. The qualitative nature of the reactions does not depend much on the chosen Hamiltonians, but there are some quantitative differences. Light

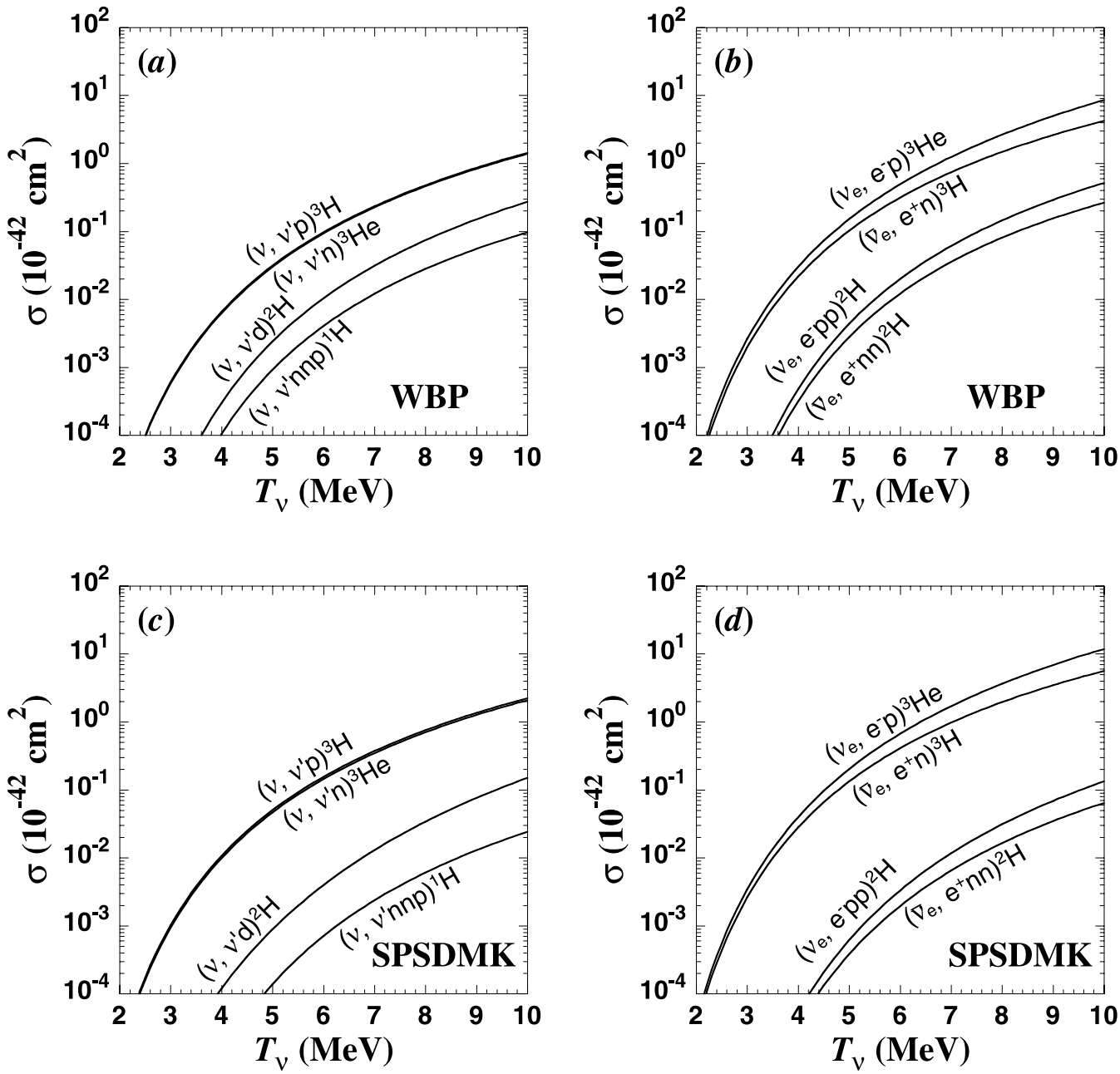

FIG. 1.—Cross sections for ^{4}He as a function of neutrino temperature T_ν. The neutrino energy spectrum is assumed to follow a Fermi-Dirac distribution with zero chemical potential. (*a*) Neutral-current reactions with the WBP Hamiltonian; (*b*) charged-current reactions with the WBP Hamiltonians; (*c*) neutral-current reactions with the SPSDMK Hamiltonian; (*d*) charged-current reactions with the SPSDMK Hamiltonian.

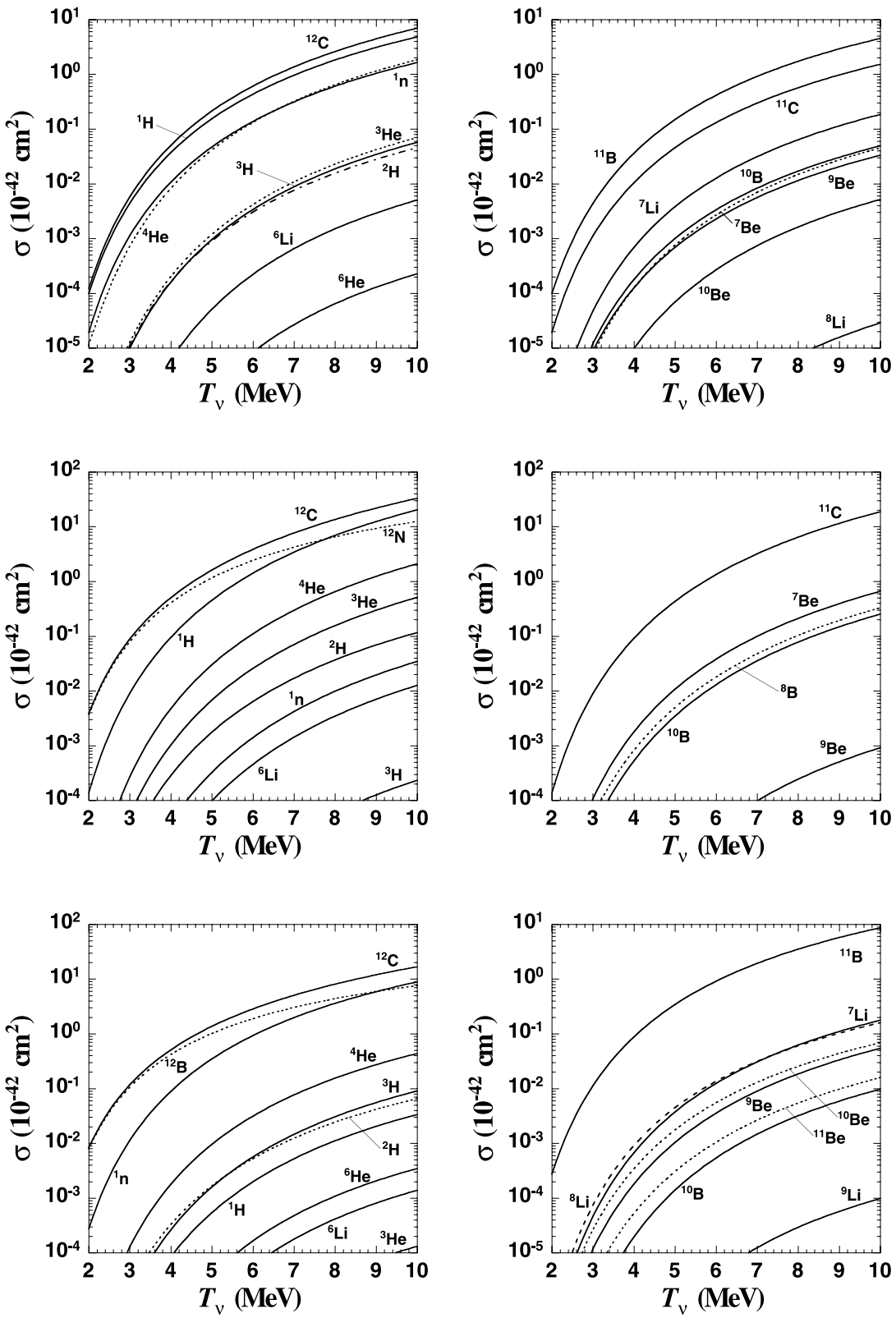

FIG. 2.—Averaged cross sections of ^{12}C as a function of neutrino temperature, T_ν, for the SFO Hamiltonian. The neutrino energy spectrum is assumed to follow a Fermi-Dirac distribution with zero chemical potential. Top, middle, and bottom panels correspond to neutral-current reactions, charged-current reactions for ν_e, and charged-current reactions for $\bar{\nu}_e$, respectively. The line labeled ^{12}C corresponds to the total decomposition rate of ^{12}C, $\sigma_{^{12}\mathrm{C},\nu}$ (see eq. [1]). [*See the electronic edition of the Journal for a color version of this figure*.]

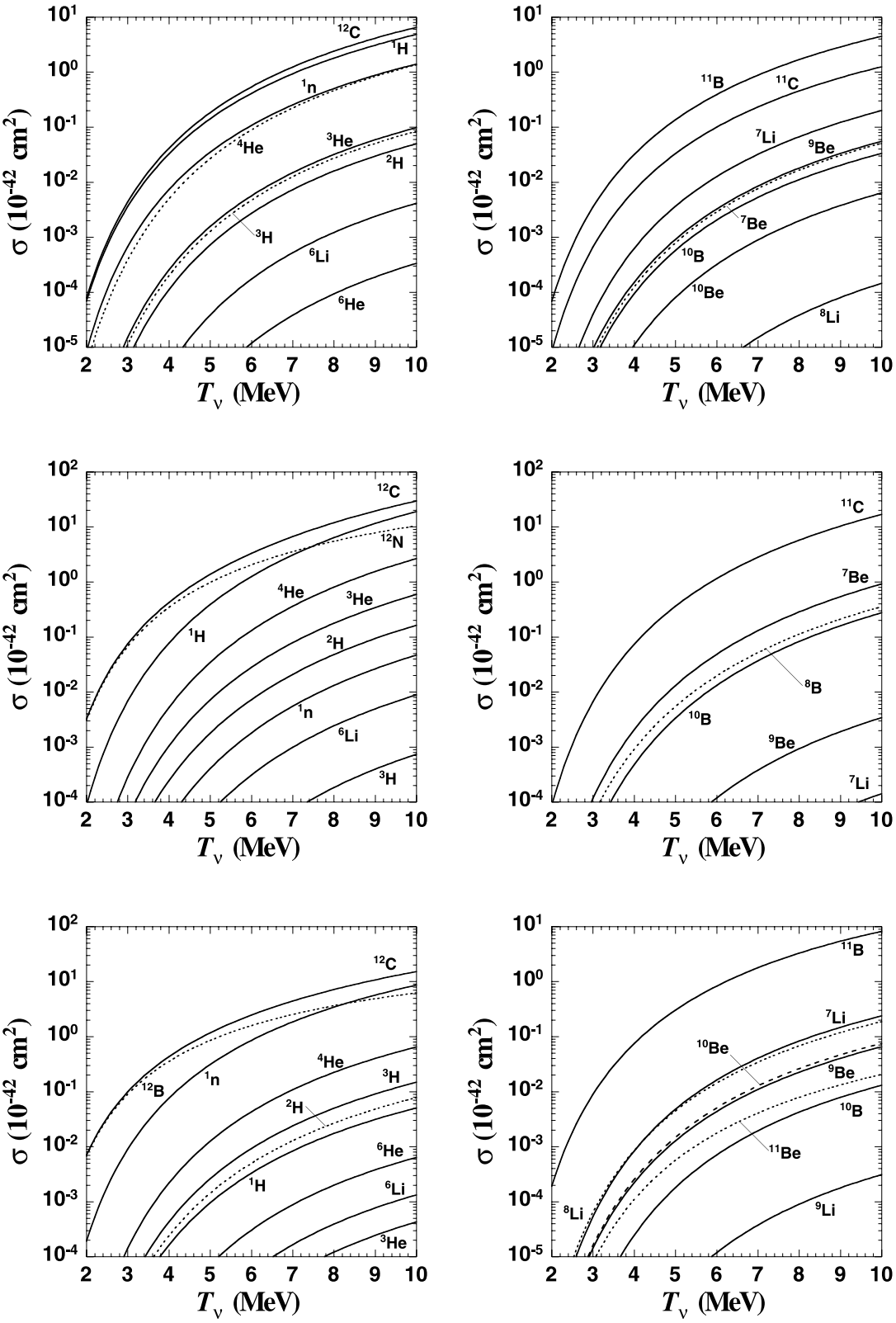

FIG. 3.—As in Fig. 2, but for the PSDMK2 Hamiltonian. [*See the electronic edition of the Journal for a color version of this figure.*]

TABLE 1

NEUTRINO-INDUCED REACTION CROSS SECTIONS OF ^{4}He IN UNITS OF 10^{-42} cm^2 USING THE WBP HAMILTONIAN

E_ν (MeV)	$(\nu,\nu' p)^3$H	$(\nu,\nu' n)^3$He	$(\nu,\nu' d)^2$H	$(\nu,\nu' nnp)^1$H	$(\nu_e,e^- p)^3$He	$(\bar{\nu}_e,e^+ n)^3$H	$(\nu_e,e^- pp)^2$H	$(\bar{\nu}_e,e^+ nn)^2$H
10.0.....	0.000E+00	0.000E+00	0.000E+00	0.000E+00	0.000E+00	0.000E+00	0.000E+00	0.000E+00
20.0.....	0.000E+00	0.000E+00	0.000E+00	0.000E+00	0.000E+00	0.000E+00	0.000E+00	0.000E+00
30.0.....	4.018E−02	3.829E−02	2.168E−11	3.538E−08	1.604E−01	1.264E−01	0.000E+00	0.000E+00
40.0.....	4.609E−01	4.425E−01	3.169E−04	9.746E−03	2.094E+00	1.556E+00	1.054E−04	1.587E−04
50.0.....	1.802E+00	1.738E+00	7.218E−02	1.730E−01	8.957E+00	5.992E+00	3.140E−01	2.211E−01
60.0.....	4.777E+00	4.620E+00	3.381E−01	7.782E−01	2.564E+01	1.529E+01	1.670E+00	1.053E+00
70.0.....	1.017E+01	9.856E+00	8.064E−01	1.991E+00	5.842E+01	3.108E+01	4.243E+00	2.409E+00
80.0.....	1.874E+01	1.818E+01	1.485E+00	4.021E+00	1.145E+02	5.453E+01	8.148E+00	4.167E+00

NOTE.—Table 1 is published in its entirety in the electronic edition of the *Astrophysical Journal*. A portion is shown here for guidance regarding its form and content.

TABLE 2

NEUTRINO-INDUCED REACTION CROSS SECTIONS OF ^{4}He IN UNITS OF 10^{-42} cm^2 USING THE SPSDMK HAMILTONIAN

E_ν (MeV)	$(\nu,\nu' p)^3$H	$(\nu,\nu' n)^3$He	$(\nu,\nu' d)^2$H	$(\nu,\nu' nnp)^1$H	$(\nu_e,e^- p)^3$He	$(\bar{\nu}_e,e^+ n)^3$H	$(\nu_e,e^- pp)^2$H	$(\bar{\nu}_e,e^+ nn)^2$H
10.0.....	0.000E+00	0.000E+00	0.000E+00	0.000E+00	0.000E+00	0.000E+00	0.000E+00	0.000E+00
20.0.....	0.000E+00	0.000E+00	0.000E+00	0.000E+00	0.000E+00	0.000E+00	0.000E+00	0.000E+00
30.0.....	6.992E−02	6.399E−02	0.000E+00	2.706E−04	2.045E−01	1.694E−01	0.000E+00	0.000E+00
40.0.....	7.360E−01	6.805E−01	3.413E−07	5.913E−03	2.709E+00	1.968E+00	0.000E+00	0.000E+00
50.0.....	2.879E+00	2.675E+00	6.340E−03	4.657E−02	1.211E+01	7.761E+00	2.338E−02	1.717E−02
60.0.....	7.633E+00	7.112E+00	5.841E−02	2.429E−01	3.557E+01	2.025E+01	2.516E−01	1.628E−01
70.0.....	1.616E+01	1.509E+01	1.800E−01	8.009E−01	8.209E+01	4.173E+01	8.673E−01	4.997E−01
80.0.....	2.944E+01	2.753E+01	3.897E−01	2.037E+00	1.614E+02	7.367E+01	2.062E+00	1.063E+00

NOTE.—Table 2 is published in its entirety in the electronic edition of the *Astrophysical Journal*. A portion is shown here for guidance regarding its form and content.

TABLE 3

NEUTRINO-INDUCED NEUTRAL-CURRENT REACTION CROSS SECTIONS OF ^{12}C IN UNITS OF 10^{-42} cm^2 BASED ON THE SFO HAMILTONIAN

E_ν (MeV)	^{12}C[a]	n	p	d	t	^{3}He	^{4}He	^{6}He	^{6}Li	^{7}Li
10.0.....	0.000E+00	0.000E+00	0.000E+00	0.000E+00	0.000E+00	0.000E+00	0.000E+00	0.000E+00	0.000E+00	0.000E+00
20.0.....	1.484E−03	1.482E−05	1.330E−03	0.000E+00	0.000E+00	0.000E+00	4.201E−04	0.000E+00	0.000E+00	0.000E+00
30.0.....	4.062E−01	8.046E−02	3.147E−01	1.329E−04	9.846E−05	1.462E−04	3.296E−02	0.000E+00	1.644E−13	5.526E−04
40.0.....	3.206E+00	7.104E−01	2.308E+00	1.259E−02	1.136E−02	1.458E−02	5.987E−01	2.569E−07	1.256E−04	5.501E−02
50.0.....	1.123E+01	2.576E+00	7.890E+00	6.209E−02	6.915E−02	8.576E−02	2.637E+00	9.178E−05	3.726E−03	2.645E−01
60.0.....	2.705E+01	6.346E+00	1.877E+01	1.765E−01	2.110E−01	2.574E−01	7.050E+00	7.484E−04	1.801E−02	7.078E−01
70.0.....	5.199E+01	1.240E+01	3.578E+01	3.657E−01	4.583E−01	5.560E−01	1.439E+01	2.094E−03	4.453E−02	1.442E+00
80.0.....	8.574E+01	2.068E+01	5.862E+01	6.252E−01	8.167E−01	9.890E−01	2.471E+01	3.979E−03	8.175E−02	2.486E+00

E_ν (MeV)	^{8}Li	^{9}Li	^{7}Be	^{9}Be	^{10}Be	^{8}B	^{10}B	^{11}B	^{10}C	^{11}C
10.0.....	0.000E+00	0.000E+00	0.000E+00	0.000E+00	0.000E+00	0.000E+00	0.000E+00	0.000E+00	0.000E+00	0.000E+00
20.0.....	0.000E+00	0.000E+00	0.000E+00	0.000E+00	0.000E+00	0.000E+00	0.000E+00	1.330E−03	0.000E+00	1.482E−05
30.0.....	0.000E+00	0.000E+00	4.367E−05	1.459E−04	7.516E−09	0.000E+00	1.331E−04	3.141E−01	0.000E+00	8.042E−02
40.0.....	0.000E+00	0.000E+00	9.063E−03	9.957E−03	5.222E−04	0.000E+00	1.386E−02	2.239E+00	5.356E−06	6.950E−01
50.0.....	1.277E−06	1.657E−12	5.537E−02	4.668E−02	5.365E−03	1.759E−08	7.018E−02	7.520E+00	1.747E−04	2.455E+00
60.0.....	6.709E−05	2.977E−08	1.657E−01	1.272E−01	1.904E−02	6.102E−06	1.920E−01	1.770E+01	9.144E−04	5.937E+00
70.0.....	2.643E−04	1.879E−07	3.596E−01	2.610E−01	4.343E−02	2.902E−05	3.891E−01	3.352E+01	2.295E−03	1.147E+01
80.0.....	5.593E−04	4.514E−07	6.455E−01	4.499E−01	7.859E−02	6.482E−05	6.616E−01	5.466E+01	4.216E−03	1.899E+01

NOTE.—Table 3 is published in its entirety in the electronic edition of the *Astrophysical Journal*. A portion is shown here for guidance regarding its form and content.

[a] Decomposition rate. See § 2 and eq. (1).

TABLE 4

NEUTRINO-INDUCED CHARGED-CURRENT REACTION CROSS SECTIONS FOR ν_e OF ^{12}C IN UNITS OF 10^{-42} cm^2 BASED ON THE SFO HAMILTONIAN

E_ν (MeV)	^{12}C[a]	n	p	d	t	^{3}He	^{4}He	^{6}Li	^{7}Li
10.0.....	0.000E+00	0.000E+00	0.000E+00	0.000E+00	0.000E+00	0.000E+00	0.000E+00	0.000E+00	0.000E+00
20.0.....	2.796E−01	0.000E+00	4.275E−05	0.000E+00	0.000E+00	0.000E+00	0.000E+00	0.000E+00	0.000E+00
30.0.....	5.516E+00	0.000E+00	5.781E−01	4.584E−07	0.000E+00	1.691E−05	9.536E−04	0.000E+00	0.000E+00
40.0.....	2.150E+01	1.330E−03	6.374E+00	2.059E−02	0.000E+00	6.608E−02	3.252E−01	1.396E−04	0.000E+00
50.0.....	5.655E+01	2.281E−02	2.658E+01	1.258E−01	2.127E−05	4.985E−01	2.159E+00	5.933E−03	6.552E−08
60.0.....	1.204E+02	1.056E−01	7.247E+01	4.043E−01	5.022E−04	1.685E+00	7.021E+00	3.680E−02	1.010E−04
70.0.....	2.209E+02	2.807E−01	1.537E+02	9.218E−01	1.981E−03	3.980E+00	1.630E+01	1.044E−01	6.282E−04
80.0.....	3.611E+02	5.595E−01	2.751E+02	1.703E+00	4.387E−03	7.625E+00	3.092E+01	2.108E−01	1.567E−03

E_ν (MeV)	^{8}Li	^{7}Be	^{9}Be	^{8}B	^{10}B	^{9}C	^{10}C	^{11}C	^{12}N
10.0.....	0.000E+00	0.000E+00	0.000E+00	0.000E+00	0.000E+00	0.000E+00	0.000E+00	0.000E+00	0.000E+00
20.0.....	0.000E+00	0.000E+00	0.000E+00	0.000E+00	0.000E+00	0.000E+00	0.000E+00	4.275E−05	2.795E−01
30.0.....	0.000E+00	1.767E−04	0.000E+00	7.430E−04	5.340E−07	0.000E+00	4.584E−07	5.779E−01	4.937E+00
40.0.....	0.000E+00	1.345E−01	6.658E−07	5.803E−02	1.235E−02	0.000E+00	2.174E−02	6.147E+00	1.506E+01
50.0.....	0.000E+00	7.781E−01	2.669E−04	3.465E−01	1.246E−01	2.064E−05	1.328E−01	2.499E+01	2.966E+01
60.0.....	2.761E−10	2.296E+00	2.518E−03	1.102E+00	4.533E−01	3.532E−04	3.996E−01	6.718E+01	4.714E+01
70.0.....	3.717E−09	5.054E+00	7.803E−03	2.556E+00	1.099E+00	1.161E−03	8.766E−01	1.413E+02	6.558E+01
80.0.....	1.062E−08	9.328E+00	1.606E−02	4.855E+00	2.136E+00	2.402E−03	1.597E+00	2.515E+02	8.314E+01

NOTE.—Table 4 is published in its entirety in the electronic edition of the *Astrophysical Journal*. A portion is shown here for guidance regarding its form and content.

[a] Decomposition rate. See § 2 and eq. (1).

elements are mainly produced by neutral current reactions induced by $\nu_{\mu,\tau}$ and $\bar{\nu}_{\mu,\tau}$, which have higher temperature than ν_e and $\bar{\nu}_e$. Note that neutral current processes involve six kinds of neutrinos.

We find that ^{11}B has the largest yield among the light elements. The branching ratio for ^{12}C$(\nu,\nu'p)^{11}$B is about 4 times larger than that for ^{12}C$(\nu,\nu'n)^{11}$C. The charged-current reaction cross section for ^{12}C$(\bar{\nu}_e,e^+n)^{11}$B at $T_{\bar{\nu}_e}=5$ MeV is nearly the same as that for ^{12}C$(\nu,\nu'n)^{11}$C at $T_\nu=6$ MeV.

^{10}B is produced mainly by neutral current reactions, ^{12}C$(\nu,\nu'pn)^{10}$B and ^{12}C$(\nu,\nu'd)^{10}$B. The amount of the production is about 6 (4) $\times 10^{-3}$ times that of ^{11}B for the SFO (PSDMK2) Hamiltonian.

^{9}Be is produced by neutral current reactions, ^{12}C$(\nu,\nu'x)^{9}$Be ($x=^3$He, dp, and ppn) and charged-current reactions, ^{12}C$(\bar{\nu}_e,e^+x)$ ^{9}Be ($x=^3$H, dn and pnn). The contribution of the latter reaction at $T_{\bar{\nu}_e}=5$ MeV is about 10% of the former at $T_\nu=6$ MeV. The

TABLE 5

NEUTRINO-INDUCED CHARGED-CURRENT REACTION CROSS SECTIONS FOR $\bar{\nu}_e$ OF ^{12}C IN UNITS OF 10^{-42} cm^2 BASED THE SFO HAMILTONIAN

E_ν (MeV)	^{12}C[a]	n	p	d	t	^{3}He	^{4}He	^{6}He	^{6}Li	^{7}Li
10.0.....	0.000E+00	0.000E+00	0.000E+00	0.000E+00	0.000E+00	0.000E+00	0.000E+00	0.000E+00	0.000E+00	0.000E+00
20.0.....	7.004E−01	5.771E−03	0.000E+00	0.000E+00	0.000E+00	0.000E+00	0.000E+00	0.000E+00	0.000E+00	0.000E+00
30.0.....	5.252E+00	8.317E−01	1.149E−05	7.809E−04	1.223E−04	0.000E+00	3.422E−03	0.000E+00	0.000E+00	8.886E−04
40.0.....	1.592E+01	5.370E+00	5.521E−03	2.646E−02	1.832E−02	0.000E+00	1.375E−01	6.683E−05	3.032E−06	5.223E−02
50.0.....	3.482E+01	1.664E+01	4.072E−02	1.090E−01	1.185E−01	5.077E−05	6.556E−01	2.976E−03	7.866E−04	2.640E−01
60.0.....	6.290E+01	3.647E+01	1.325E−01	2.743E−01	3.579E−01	4.628E−04	1.759E+00	1.404E−02	5.310E−03	7.095E−01
70.0.....	9.941E+01	6.470E+01	2.854E−01	5.194E−01	7.521E−01	1.296E−03	3.494E+00	3.240E−02	1.341E−02	1.419E+00
80.0.....	1.422E+02	9.948E+01	4.916E−01	8.266E−01	1.290E+00	2.367E−03	5.803E+00	5.553E−02	2.362E−02	2.379E+00

E_ν (MeV)	^{8}Li	^{9}Li	^{7}Be	^{9}Be	^{10}Be	^{11}Be	^{10}B	^{11}B	^{12}B
10.0.....	0.000E+00	0.000E+00	0.000E+00	0.000E+00	0.000E+00	0.000E+00	0.000E+00	0.000E+00	0.000E+00
20.0.....	0.000E+00	0.000E+00	0.000E+00	0.000E+00	0.000E+00	0.000E+00	0.000E+00	5.771E−03	6.946E−01
30.0.....	2.533E−03	0.000E+00	0.000E+00	1.223E−04	7.809E−04	1.149E−05	1.220E−16	8.309E−01	4.417E+00
40.0.....	7.545E−02	0.000E+00	0.000E+00	1.361E−02	2.765E−02	4.090E−03	8.826E−04	5.310E+00	1.044E+01
50.0.....	2.821E−01	5.011E−05	5.056E−12	7.359E−02	1.164E−01	2.238E−02	1.154E−02	1.627E+01	1.772E+01
60.0.....	6.551E−01	3.794E−04	3.581E−07	2.125E−01	2.872E−01	6.241E−02	4.018E−02	3.537E+01	2.536E+01
70.0.....	1.206E+00	9.657E−04	1.865E−06	4.418E−01	5.389E−01	1.282E−01	8.540E−02	6.241E+01	3.273E+01
80.0.....	1.922E+00	1.693E−03	4.074E−06	7.559E−01	8.586E−01	2.189E−01	1.438E−01	9.560E+01	3.950E+01

NOTE.—Table 5 is published in its entirety in the electronic edition of the *Astrophysical Journal*. A portion is shown here for guidance regarding its form and content.

[a] Decomposition rate. See § 2 and eq. (1).

TABLE 6

NEUTRINO-INDUCED NEUTRAL-CURRENT REACTION CROSS SECTIONS OF ^{12}C IN UNITS OF 10^{-42} cm^2 BASED ON THE PSDMK2 HAMILTONIAN

E_ν (MeV)	^{12}C[a]	n	p	d	t	^{3}He	^{4}He	^{6}He	^{6}Li	^{7}Li
10.0.....	0.000E+00	0.000E+00	0.000E+00	0.000E+00	0.000E+00	0.000E+00	0.000E+00	0.000E+00	0.000E+00	0.000E+00
20.0.....	3.289E−04	2.518E−07	2.648E−04	0.000E+00	0.000E+00	0.000E+00	1.914E−04	0.000E+00	0.000E+00	0.000E+00
30.0.....	2.976E−01	4.222E−02	2.504E−01	4.759E−06	3.311E−05	1.551E−04	1.481E−02	0.000E+00	1.826E−24	3.170E−04
40.0.....	2.730E+00	5.182E−01	2.114E+00	7.058E−03	1.314E−02	1.741E−02	3.537E−01	1.316E−07	3.610E−05	4.747E−02
50.0.....	1.016E+01	2.077E+00	7.658E+00	5.211E−02	9.507E−02	1.138E−01	1.778E+00	9.817E−05	2.592E−03	2.633E−01
60.0.....	2.526E+01	5.382E+00	1.881E+01	1.827E−01	3.082E−01	3.575E−01	5.089E+00	1.037E−03	1.452E−02	7.470E−01
70.0.....	4.950E+01	1.081E+01	3.657E+01	4.194E−01	6.883E−01	7.909E−01	1.079E+01	3.135E−03	3.761E−02	1.571E+00
80.0.....	8.259E+01	1.833E+01	6.067E+01	7.514E−01	1.242E+00	1.423E+00	1.894E+01	6.070E−03	6.935E−02	2.765E+00

E_ν (MeV)	^{8}Li	^{9}Li	^{7}Be	^{9}Be	^{10}Be	^{8}B	^{10}B	^{11}B	^{10}C	^{11}C
10.0.....	0.000E+00	0.000E+00	0.000E+00	0.000E+00	0.000E+00	0.000E+00	0.000E+00	0.000E+00	0.000E+00	0.000E+00
20.0.....	0.000E+00	0.000E+00	0.000E+00	0.000E+00	0.000E+00	0.000E+00	0.000E+00	2.648E−04	0.000E+00	2.518E−07
30.0.....	0.000E+00	0.000E+00	3.331E−06	1.525E−04	3.542E−09	0.000E+00	4.759E−06	2.501E−01	0.000E+00	4.221E−02
40.0.....	0.000E+00	0.000E+00	8.400E−03	1.041E−02	4.961E−04	0.000E+00	6.689E−03	2.050E+00	4.332E−06	5.005E−01
50.0.....	1.008E−05	2.562E−13	5.944E−02	6.500E−02	6.162E−03	1.030E−08	4.242E−02	7.248E+00	2.332E−04	1.929E+00
60.0.....	3.630E−04	6.660E−08	1.857E−01	2.028E−01	2.324E−02	1.494E−05	1.278E−01	1.753E+01	1.294E−03	4.860E+00
70.0.....	1.361E−03	5.621E−07	4.095E−01	4.464E−01	5.411E−02	7.867E−05	2.698E−01	3.374E+01	3.327E−03	9.602E+00
80.0.....	2.812E−03	1.436E−06	7.399E−01	7.994E−01	9.837E−02	1.795E−04	4.658E−01	5.561E+01	6.111E−03	1.612E+01

NOTE.—Table 6 is published in its entirety in the electronic edition of the *Astrophysical Journal*. A portion is shown here for guidance regarding its form and content.

[a] Decomposition rate. See § 2 and eq. (1).

production of ^{9}Be is about 4 (7) $\times 10^{-3}$ times that of ^{11}B for the SFO (PSDMK2) Hamiltonian.

For ^{10}Be, charged-current reaction cross sections for ^{12}C $(\bar{\nu}_e, e^+pn)$ ^{10}Be and ^{12}C $(\bar{\nu}_e, e^+d)$ ^{10}Be are larger than neutral current reaction cross section for ^{12}C $(\nu, \nu' pp)$ ^{10}Be at $(T_{\bar{\nu}_e}, T_\nu) =$ (5 MeV, 6 MeV), while at $T_{\bar{\nu}_e} = 4$ MeV the former is as small as one-fourth of the latter. Production yields of ^{10}Be, thus, depend on $T_{\bar{\nu}_e}$. The production of ^{10}Be by neutral current processes is about 5 (6) $\times 10^{-4}$ times that of ^{11}B for the SFO (PSDMK2) case.

^{7}Li is mainly produced by neutral current reactions, ^{12}C $(\nu, \nu' p\alpha)^7$Li, etc. The production of ^{7}Li through ^{7}Be is about 20% of that from the neutral current reactions. Contributions from charged-current processes are less than 10% of those from the neutral current reactions at $T_{\bar{\nu}_e} = 5$ MeV. ^{6}Li is produced by neutral current processes, but production through ^{6}He is negligible.

TABLE 7

NEUTRINO-INDUCED CHARGED-CURRENT REACTION CROSS SECTIONS FOR ν_e OF ^{12}C IN UNITS OF 10^{-42} cm^2 BASED ON THE PSDMK2 HAMILTONIAN

E_ν (MeV)	^{12}C[a]	n	p	d	t	^{3}He	^{4}He	^{6}Li	^{7}Li
10.0.....	0.000E+00	0.000E+00	0.000E+00	0.000E+00	0.000E+00	0.000E+00	0.000E+00	0.000E+00	0.000E+00
20.0.....	2.363E−01	0.000E+00	2.663E−06	0.000E+00	0.000E+00	0.000E+00	0.000E+00	0.000E+00	0.000E+00
30.0.....	4.557E+00	0.000E+00	3.901E−01	1.076E−06	0.000E+00	6.638E−05	1.909E−03	0.000E+00	0.000E+00
40.0.....	1.802E+01	1.183E−03	5.282E+00	1.233E−02	0.000E+00	5.975E−02	3.247E−01	3.825E−05	0.000E+00
50.0.....	4.884E+01	2.703E−02	2.365E+01	1.266E−01	3.300E−05	5.269E−01	2.478E+00	3.558E−03	1.215E−07
60.0.....	1.071E+02	1.370E−01	6.690E+01	5.133E−01	1.394E−03	1.897E+00	8.601E+00	2.519E−02	1.707E−04
70.0.....	2.011E+02	3.824E−01	1.450E+02	1.313E+00	6.217E−03	4.621E+00	2.065E+01	7.503E−02	1.126E−03
80.0.....	3.346E+02	7.755E−01	2.632E+02	2.567E+00	1.418E−02	8.990E+00	3.981E+01	1.523E−01	2.829E−03

E_ν (MeV)	^{8}Li	^{7}Be	^{9}Be	^{8}B	^{10}B	^{9}C	^{10}C	^{11}C	^{12}N
10.0.....	0.000E+00	0.000E+00	0.000E+00	0.000E+00	0.000E+00	0.000E+00	0.000E+00	0.000E+00	0.000E+00
20.0.....	0.000E+00	0.000E+00	0.000E+00	0.000E+00	0.000E+00	0.000E+00	0.000E+00	2.663E−06	2.363E−01
30.0.....	0.000E+00	7.641E−04	0.000E+00	1.012E−03	6.827E−06	0.000E+00	1.076E−06	3.892E−01	4.166E+00
40.0.....	0.000E+00	1.398E−01	1.573E−05	6.329E−02	1.358E−02	0.000E+00	1.245E−02	5.052E+00	1.268E+01
50.0.....	0.000E+00	9.564E−01	1.355E−03	3.774E−01	1.405E−01	3.162E−05	1.102E−01	2.176E+01	2.493E+01
60.0.....	4.085E−09	3.061E+00	9.674E−03	1.201E+00	5.190E−01	8.437E−04	3.828E−01	6.016E+01	3.953E+01
70.0.....	9.469E−08	7.057E+00	2.881E−02	2.776E+00	1.262E+00	3.024E−03	9.070E−01	1.287E+02	5.488E+01
80.0.....	2.948E−07	1.339E+01	5.859E−02	5.242E+00	2.442E+00	6.394E−03	1.733E+00	2.315E+02	6.945E+01

NOTE.—Table 7 is published in its entirety in the electronic edition of the *Astrophysical Journal*. A portion is shown here for guidance regarding its form and content.

[a] Decomposition rate. See § 2 and eq. (1).

TABLE 8
NEUTRINO-INDUCED CHARGED-CURRENT REACTION CROSS SECTIONS FOR $\bar{\nu}_e$ OF ^{12}C IN UNITS OF 10^{-42} cm^2 BASED ON THE PSDMK2 HAMILTONIAN

E_ν (MeV)	^{12}C[a]	n	p	d	t	^{3}He	^{4}He	^{6}He	^{6}Li	^{7}Li
10.0.....	0.000E+00	0.000E+00	0.000E+00	0.000E+00	0.000E+00	0.000E+00	0.000E+00	0.000E+00	0.000E+00	0.000E+00
20.0.....	5.917E−01	2.368E−03	0.000E+00	0.000E+00	0.000E+00	0.000E+00	0.000E+00	0.000E+00	0.000E+00	0.000E+00
30.0.....	4.382E+00	6.548E−01	2.563E−05	5.835E−05	6.821E−05	0.000E+00	1.867E−03	0.000E+00	0.000E+00	1.566E−04
40.0.....	1.363E+01	4.810E+00	1.195E−02	1.714E−02	3.012E−02	0.000E+00	1.608E−01	1.324E−04	1.989E−06	6.479E−02
50.0.....	3.079E+01	1.571E+01	6.777E−02	1.026E−01	1.932E−01	1.069E−04	8.939E−01	5.357E−03	5.897E−04	3.480E−01
60.0.....	5.724E+01	3.543E+01	2.043E−01	3.160E−01	5.845E−01	1.392E−03	2.582E+00	2.564E−02	4.866E−03	9.508E−01
70.0.....	9.248E+01	6.393E+01	4.246E−01	6.618E−01	1.227E+00	4.247E−03	5.325E+00	6.002E−02	1.306E−02	1.914E+00
80.0.....	1.344E+02	9.928E+01	7.099E−01	1.109E+00	2.095E+00	7.954E−03	8.998E+00	1.028E−01	2.338E−02	3.218E+00

E_ν (MeV)	^{8}Li	^{9}Li	^{7}Be	^{9}Be	^{10}Be	^{11}Be	^{10}B	^{11}B	^{12}B
10.0.....	0.000E+00	0.000E+00	0.000E+00	0.000E+00	0.000E+00	0.000E+00	0.000E+00	0.000E+00	0.000E+00
20.0.....	0.000E+00	0.000E+00	0.000E+00	0.000E+00	0.000E+00	0.000E+00	0.000E+00	2.368E−03	5.893E−01
30.0.....	1.687E−03	0.000E+00	0.000E+00	5.622E−05	5.844E−05	2.555E−05	1.521E−08	6.546E−01	3.726E+00
40.0.....	6.814E−02	0.000E+00	0.000E+00	1.674E−02	1.892E−02	9.553E−03	9.832E−04	4.727E+00	8.713E+00
50.0.....	2.989E−01	1.056E−04	5.199E−12	9.082E−02	1.084E−01	3.839E−02	1.462E−02	1.516E+01	1.461E+01
60.0.....	7.605E−01	1.117E−03	1.744E−06	2.612E−01	3.058E−01	8.812E−02	5.364E−02	3.373E+01	2.064E+01
70.0.....	1.478E+00	3.086E−03	1.104E−05	5.345E−01	6.164E−01	1.578E−01	1.161E−01	6.031E+01	2.635E+01
80.0.....	2.424E+00	5.555E−03	2.528E−05	8.968E−01	1.027E+00	2.440E−01	1.955E−01	9.311E+01	3.154E+01

NOTE.—Table 8 is published in its entirety in the electronic edition of the *Astrophysical Journal*. A portion is shown here for guidance regarding its form and content.

[a] Decomposition rate. See § 2 and eq. (1).

Light-element synthesis during supernova explosions based on the present reaction cross sections is discussed in § 4.

3. SN NUCLEOSYNTHESIS MODEL

In this study, we adopt the same SN nucleosynthesis model employed by Yoshida et al. (2006a, 2006b), except for the new ν-process reaction rates. Here we briefly explain the SN explosion model, the SN neutrino model, and the nuclear reaction network.

3.1. *SN Explosion Model*

We consider a 16.2 $M_\odot$ presupernova model, corresponding to a possible progenitor model for SN 1987A (Shigeyama & Nomoto 1990). The explosion is proceeded by a spherically symmetric hydrodynamic calculation using a piecewise parabolic method code (Colella & Woodward 1984; Shigeyama et al. 1992). The explosion energy is set to be 1 B = 1 Bethe = 1×10^{51} ergs. The Lagrangian location of the mass cut is fixed at 1.61 $M_\odot$.

For calculations of the effects of neutrino oscillations, we use the density profile of the presupernova model. As discussed in Yoshida et al. (2006b), shock propagation hardly affects the ν-process (with neutrino oscillations). There is a resonance of the transition of 2–3 mass eigenstates in the O/C layer. When the shock wave arrives at this resonance region, the density gradient becomes large, and therefore the resonance becomes nonadiabatic. If the adiabaticity is changed by the shock wave, the influence of neutrino oscillations could change as well. However, most of the supernova neutrinos have already passed this region before the shock arrives, so that the affected fraction of neutrinos is very small.

3.2. *SN Neutrino Model*

Here, we briefly explain models for the flux and energy spectra of the neutrinos emitted from the neutrino sphere. For simplicity, we assume that the neutrino luminosity decreases exponentially with a decay time of $\tau_\nu = 3$ s. The total energy carried out by neutrinos is almost equal to the binding energy released at the formation of a proto–neutron star. A characteristic value of the energy is 3×10^{53} ergs (e.g., Woosley et al. 1990), corresponding to the gravitational binding energy of a 1.4 $M_\odot$ neutron star (Lattimer & Yahil 1989; Lattimer & Prakash 2001). The spectra at the neutrino sphere are assumed to follow Fermi-Dirac distributions with zero chemical potentials. Note that the temperatures of neutrinos and the total neutrino energy are somewhat uncertain, and that the ^{11}B abundance in GCE can be used to constrain them.

We consider several neutrino models, parameterized by the neutrino temperatures, total energy released in neutrinos, and adopted cross sections. Table 9 lists seven models employed in this study. We use model 1 as the "standard model" in this study, with $T_{\nu_e} = 3.2$ MeV, $T_{\bar{\nu}_e} = 5.0$ MeV, $T_{\nu_{\mu,\tau}} = 6.0$ MeV, and $E_{\nu,\mathrm{total}} = 3.0 \times 10^{53}$ ergs, where T_{ν_e}, $T_{\bar{\nu}_e}$, $T_{\nu_{\mu,\tau}}$, and $E_{\nu,\mathrm{total}}$ are the temperatures of e-neutrinos, e-antineutrinos, μ- and τ-neutrinos and their antiparticles, and the total neutrino energy. This set of the neutrino temperatures and total neutrino energy were used in the standard model of Yoshida et al. (2004, 2005a, 2006a, 2006b). This model adopts the cross sections of ^{12}C and ^{4}He from SFO and WBP Hamiltonians, respectively.

Models 1mk, 1p, and 1hw have the same set of the neutrino temperatures and total neutrino energy as in model 1, but adopt different sets of ^{12}C and ^{4}He cross sections. Model 1mk adopts the cross sections of ^{12}C and ^{4}He with PSDMK2 and SPSDMK Hamiltonians (Tables 1*c*, 1*d*, 6–8). Model 1p contains the cross sections of $^{4}\mathrm{He}(\nu,\nu'p)^{3}\mathrm{H}$, $^{4}\mathrm{He}(\nu,\nu'n)^{3}\mathrm{He}$, $^{4}\mathrm{He}(\nu_e,e^-p)^{3}\mathrm{He}$, and $^{4}\mathrm{He}(\bar{\nu}_e,e^+n)^{3}\mathrm{H}$ for ^{4}He, and $^{12}\mathrm{C}(\nu,\nu'p)^{11}\mathrm{B}$, $^{12}\mathrm{C}(\nu,\nu'n)^{11}\mathrm{C}$, $^{12}\mathrm{C}(\nu_e,e^-p)^{11}\mathrm{C}$, and $^{12}\mathrm{C}(\bar{\nu}_e,e^+n)^{11}\mathrm{B}$ for ^{12}C evaluated in Suzuki et al. (2006). Since the reaction rates of $^{12}\mathrm{C}(\nu,\nu'np)^{10}\mathrm{B}$, $^{12}\mathrm{C}(\nu,\nu'^{3}\mathrm{He})^{9}\mathrm{Be}$, $^{12}\mathrm{C}(\nu,\nu'p\alpha)^{7}\mathrm{Li}$, and $^{12}\mathrm{C}(\nu,\nu'n\alpha)^{7}\mathrm{Be}$ were not evaluated in Suzuki et al. (2006), the rates of these reactions are adopted from HW92. Model 1hw is equivalent to the standard model in Yoshida et al. (2006b). It adopts the cross sections of ^{4}He and ^{12}C from HW92. Model 2 represents the same neutrino energy spectra as used in Rauscher et al. (2002), Heger et al. (2005), and Yoshida et al. (2005b, 2007, 2008).

TABLE 9
Model Parameters

Model	T_{ν_e} (MeV)	$T_{\bar{\nu}_e}$ (MeV)	$T_{\nu_{\mu,\tau}}$ (MeV)	$E_{\nu,\mathrm{total}}$ ($\times 10^{53}$ ergs)	References for ^{12}C and ^{4}He ν−Process
Model 1	3.2	5.0	6.0	3.0	SFO, WBP
Model 1mk	3.2	5.0	6.0	3.0	PSDMK2, SPSDMK
Model 1p	3.2	5.0	6.0	3.0	SFO,[a] WBP,[a] HW92
Model 1hw	3.2	5.0	6.0	3.0	HW92
Model 2	4.0	4.0	6.0	3.0	SFO, WBP
Model LT	3.2	5.0	6.5	2.35	SFO, WBP
Model ST	3.2	4.2	5.0	3.53	SFO, WBP

Note.—Neutrino temperatures T_{ν_e}, $T_{\bar{\nu}_e}$, $T_{\nu_{\mu,\tau}}$, total released neutrino energy $E_{\nu,\mathrm{total}}$, and adopted neutrino-nucleus cross sections for ^{12}C and ^{4}He.
[a] Suzuki et al. (2006).

When we investigate the effects of neutrino oscillations on SN nucleosynthesis, we consider two additional sets, to take into account uncertainties in neutrino temperatures. Model LT corresponds to the largest $T_{\nu_{\mu,\tau}}$ value and indicates the ^{11}B yield close to the upper limit still satisfying GCE constraints (Fields et al. 2000; Ramaty et al. 2000a, 2000b; Alibés et al. 2002). Model ST corresponds to the smallest $T_{\nu_{\mu,\tau}}$ value and indicates the value close to the lower limit deduced from GCE models. We note that the temperature of $\bar{\nu}_e$ in model ST is changed to keep $T_{\nu_{\mu,\tau}}/T_{\bar{\nu}_e} \sim 1.2$, which is the same as model 1.

When neutrino oscillations are taken into account, the neutrinos emitted from the neutrino sphere change flavor in passing through the stellar interior. The flavor change depends strongly on neutrino oscillation parameters. We use the following values for these parameters. The squared-mass differences of the mass eigenstates $\Delta m_{ij}^2 = m_i^2 - m_j^2$ are set to be

$$\Delta m_{21}^2 = 7.9 \times 10^{-5} \quad \mathrm{eV}^2$$
$$\left|\Delta m_{31}^2\right| = 2.4 \times 10^{-3} \quad \mathrm{eV}^2. \tag{2}$$

The values of the mixing angles θ_{12} and θ_{23} are fixed to be

$$\sin^2 2\theta_{12} = 0.816, \qquad \sin^2 2\theta_{23} = 1. \tag{3}$$

These parameter values correspond to the family of the so-called large mixing angle (LMA) solutions, determined with Super-Kamiokande (Ashie et al. 2004), SNO (Sudbury Neutrino Observatory; Ahmed et al. 2004), and KamLAND (Araki et al. 2005). In the case of Δm_{31}^2, only the absolute value has been determined. The positive and negative values correspond to normal and inverted mass hierarchies, respectively. For the mixing angle θ_{13}, the upper limit of $\sin^2 2\theta_{13}$ has been determined to be $\sin^2 2\theta_{13} \sim 0.1$ from the CHOOZ experiment (Apollonio et al. 2003). In this study, we use values of $\sin^2 2\theta_{13}$ between 1×10^{-6} and 0.1.

There are two resonances in the transitions between two mass eigenstates in the stellar interior of the presupernova. The resonance density is obtained from

$$\rho_{\mathrm{res}} Y_e = \frac{m_u \Delta m_{ji}^2 c^4 \cos 2\theta_{ij}}{2\sqrt{2} G_{\mathrm{F}} (\hbar c)^3 \varepsilon_\nu}$$
$$= 6.55 \times 10^6 \left(\frac{\Delta m_{ji}^2}{1\ \mathrm{eV}^2}\right)\left(\frac{1\ \mathrm{MeV}}{\varepsilon_\nu}\right) \cos 2\theta_{ij}\ \mathrm{g\ cm^{-3}}, \tag{4}$$

where ρ_{res} is the resonance density, Y_e is the electron fraction, m_u is the atomic mass unit, c is the speed of light, G_{F} is the Fermi constant, $\hbar$ is the Planck constant divided by 2π, and ε_ν is the neutrino energy.

One resonance is related to the transition between the 2–3 mass eigenstates. We refer to this resonance as the "H resonance". The density range of the H resonance is $\rho_{\mathrm{res}} \sim 300$–$3000$ g cm^{-3}, with the energy range of $\varepsilon_\nu \sim 10$–100 MeV. This density range corresponds to the C/O layer and the inner region of the He layer. Adiabaticity of the H resonance depends on the value of the oscillation parameter $\sin^2 2\theta_{13}$.

The other resonance is due to the transition between the 1 and 2 mass eigenstates. We refer to this resonance as the "L resonance." The density range of the L resonance is $\rho_{\mathrm{res}} \sim 4$–$40$ g cm^{-3}. The location of the L resonance is in the He layer. The L resonance is an adiabatic resonance in the range of neutrino oscillation parameters considered in this study. Details of neutrino oscillations in this supernova model are provided in Yoshida et al. (2006b).

3.3. *Nucleosynthesis Model*

We calculate the nucleosynthesis of the supernova explosion using a nuclear reaction network consisting of 291 nuclear species, as used in Yoshida et al. (2004, 2005a, 2006a, 2006b) and tabulated in Table 1 in Yoshida et al. (2004). The difference from previous studies (Yoshida et al. 2006a, 2006b) is that here new cross sections for neutrino-^{12}C and neutrino-^{4}He reactions are used (see § 2). Reaction rates are calculated using these new cross sections and the neutrino energy spectra discussed above. When we take neutrino oscillations into account, the formulation of the rates of the charged-current ν-process reactions is given by equation (8) in Yoshida et al. (2006b). The range of the neutrino energy for integration is capped at 160 MeV. The reaction rates of the other ν-process reactions are adopted from HW92, and the effects of neutrino oscillations are not included for those reactions.

4. LIGHT ELEMENT YIELDS

4.1. *Production of Light Elements in SNe*

Below we discuss the production processes of light elements in the SN model with the new cross sections for ^{4}He and ^{12}C. The mass fraction distribution of the light elements at 1000 s after core bounce is shown in Figure 4. The mass fractions of ^{7}Li and ^{11}B are larger than those of other light elements. The third abundant species is ^{10}B. The abundances of ^{6}Li and ^{9}Be are smaller than that of ^{10}B by more than an order of magnitude. The radioactive isotope ^{10}Be is produced at a level similar to those of ^{6}Li and ^{9}Be.

4.1.1. ^{7}Li

Most of ^{7}Li is produced in the He/C layer. The ^{7}Li is originally produced as ^{7}Li and its isobar ^{7}Be. In an inner region of the He/C

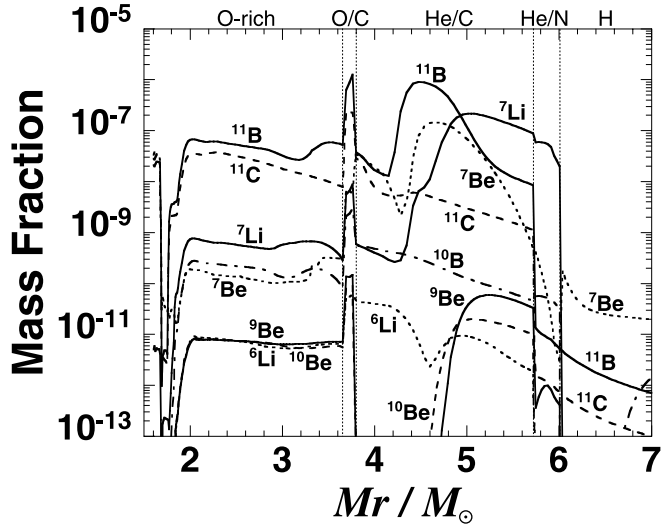

FIG. 4.—Mass fraction distributions for model 1. Blue solid and dashed lines correspond to the mass fractions of ^{7}Li and ^{7}Be, respectively. Red solid and dashed lines are the mass fractions of ^{11}B and ^{11}C. [*See the electronic edition of the Journal for a color version of this figure.*]

layer ($M_r \lesssim 4.8\ M_\odot$), the production of ^{7}Be dominates. Most of ^{7}Be is produced through $^{4}\mathrm{He}(\nu, \nu' n)^{3}\mathrm{He}$ and $^{3}\mathrm{He}(\alpha, \gamma)^{7}\mathrm{Be}$. The charged-current reaction $^{4}\mathrm{He}(\nu_e, e^- p)^{3}\mathrm{He}$ contributes less to the ^{7}Be production, but is important when neutrino oscillations are considered (see § 5). In the O/Ne layer, the mass fraction of ^{7}Be is small. Most of ^{7}Be is produced through the ν-process of ^{12}C. When the shock wave arrives, almost all the ^{7}Be is photodisintegrated by $^{7}\mathrm{Be}(\gamma, \alpha)^{3}\mathrm{He}$. During the expansion stage, ^{7}Be is again produced from ^{12}C.

In the outer region of the He/C layer, most of ^{7}Li is produced via the reaction sequence $^{4}\mathrm{He}(\nu, \nu' p)^{3}\mathrm{H}(\alpha, \gamma)^{7}\mathrm{Li}$. Some of ^{7}Li is contributed by the charged-current reaction $^{4}\mathrm{He}(\bar{\nu}_e, e^+ n)^{3}\mathrm{H}$. In this region, all ^{3}H produced through the ν-process is consumed by α-capture to ^{7}Li during the explosion. On the other hand, a much smaller amount of ^{7}Be is produced, because the shock temperature is too low to effectively enable $^{3}\mathrm{He}(\alpha, \gamma)^{7}\mathrm{Be}$ during the explosion. In the inner region of the He/C layer, the produced ^{7}Li experiences α-capture to yield ^{11}B during the explosion. In the O-rich layer, ^{7}Li is produced through the ν-process of ^{12}C, and further α-capture produces ^{11}B.

4.1.2. ^{11}B

About 60% of ^{11}B is produced in the He/C layer. Most of the ^{11}B is produced through $^{7}\mathrm{Li}(\alpha, \gamma)^{11}\mathrm{B}$ in the mass coordinate range $4.2\ M_\odot \lesssim M_r \lesssim 4.9\ M_\odot$. In this region, the mass fraction of ^{7}Li becomes very small owing to this reaction (see Fig. 4). A very small amount of the isobar ^{11}C is coproduced through $^{12}\mathrm{C}(\nu, \nu' n)^{11}\mathrm{C}$.

In the O-rich layer (O/Ne and O/C layers), both ^{11}B and ^{11}C are produced through the ν-process of ^{12}C. The sum of their mass fractions is about 10^{-6} in the O/C layer, because the mass fraction of ^{12}C is also large. The mass fractions of ^{11}B and ^{11}C are similar about 10 s after the explosion. Some ^{11}B is destroyed by $^{11}\mathrm{B}(\alpha, p)^{14}\mathrm{C}$. In the O/Ne layer, ^{11}B is produced as ^{11}C. The branching ratio of ^{11}B is larger than that of ^{11}C in the ν-process of ^{12}C. Therefore, the amount of ^{11}B produced through the ν-process is larger than the amount of ^{11}C. However, more than 90% of ^{11}B is lost due to the reaction $^{11}\mathrm{B}(\alpha, p)^{14}\mathrm{C}$ at shock arrival. The ν-process that continues after the explosion increases the ^{11}B abundance again, but to a lesser extent than ^{11}C. The main destruction reaction of ^{11}C is $^{11}\mathrm{C}(\alpha, p)^{14}\mathrm{N}$, but it is practically negligible. The produced ^{11}C decays to ^{11}B by β^+-decay and electron capture with a half-life of 20.39 minutes. Thus, the mass fraction of ^{11}B in the O-rich layer is larger than that of ^{11}C in Figure 4.

4.1.3. ^{6}Li *and* ^{9}Be

The production processes of ^{6}Li and ^{9}Be are connected. About 65% and 60% of ^{6}Li and ^{9}Be, respectively, are produced in the He/C layer. Most of ^{9}Be is produced through the ν-process reaction $^{12}\mathrm{C}(\nu, \nu' x)^{9}\mathrm{Be}$. However, it is decomposed after shock arrival at $M_r \lesssim 5.0\ M_\odot$. The main destructive reaction is $^{9}\mathrm{Be}(\alpha, n)^{12}\mathrm{C}$. About a half of ^{6}Li is produced through $^{4}\mathrm{He}(\nu, \nu' d)^{2}\mathrm{H}(\alpha, \gamma)^{6}\mathrm{Li}$ in the region $3.8\ M_\odot \lesssim M_r \lesssim 4.6\ M_\odot$ in the He/C layer. Additional ^{6}Li is synthesized through $^{12}\mathrm{C}(\nu, \nu' x)^{6}\mathrm{Li}$ before shock arrival and through $^{9}\mathrm{Be}(p, \alpha)^{6}\mathrm{Li}$ after shock arrival. In the inner region of the He/C layer ^{6}Li is destroyed through $^{6}\mathrm{Li}(p, \alpha)^{3}\mathrm{He}$.

In the O-rich layer, ^{9}Be is mainly produced through $^{12}\mathrm{C}(\nu, \nu' x)^{9}\mathrm{Be}$. Almost all of the ^{9}Be produced before shock arrival is destroyed completely through $^{9}\mathrm{Be}(\alpha, n)^{12}\mathrm{C}$ by the shock. It is supplied again through $^{12}\mathrm{C}(\nu, \nu' x)^{9}\mathrm{Be}$ during the expansion stage. It is partly produced through $^{12}\mathrm{C}(\bar{\nu}_e, e^+)^{12}\mathrm{B}(p, \alpha)^{9}\mathrm{Be}$. In this layer, the main production process for ^{6}Li is $^{9}\mathrm{Be}(p, \alpha)^{6}\mathrm{Li}$. This reaction is effective even before shock arrival. The temperature increase from the shock reduces the ^{6}Li abundance through $^{6}\mathrm{Li}(p, \alpha)^{3}\mathrm{He}$. However, ^{6}Li is supplied again via $^{9}\mathrm{Be}(p, \alpha)^{6}\mathrm{Li}$ during postshock expansion. The contribution from $^{12}\mathrm{C}(\nu, \nu' x)^{6}\mathrm{Li}$ is small.

4.1.4. ^{10}Be

Radioactive ^{10}Be is produced in both the O-rich and He/C layers. It is mainly produced through the charged-current reaction $^{12}\mathrm{C}(\bar{\nu}_e, e^+ x)^{10}\mathrm{Be}$ and the neutral-current reaction $^{12}\mathrm{C}(\nu, \nu' x)^{10}\mathrm{Be}$. The contribution from the charged-current reaction is larger than that from the neutral-current reaction in this model. The produced ^{10}Be is destroyed by $^{10}\mathrm{Be}(\alpha, n)^{13}\mathrm{C}$ at shock arrival at $M_r \lesssim 4.8\ M_\odot$. In the O-rich layer, however, the ν-process reaction still increases the ^{10}Be amount during the expansion stage. We note that the ν-process reactions producing ^{10}Be directly are included in this study for the first time. When we do not include these reactions, ^{10}Be is produced through $^{12}\mathrm{C}(\bar{\nu}_e, e^+ p)^{11}\mathrm{Be}(\gamma, n)^{10}\mathrm{Be}$.

4.1.5. ^{10}B

About 80% of the ^{10}B amount is produced through the ν-process of ^{12}C, mainly via $^{12}\mathrm{C}(\nu, \nu' x)^{10}\mathrm{B}$. About a half of ^{10}B is produced in the O-rich (O/Ne and O/C) layer. In the O-rich layer, some ^{10}B is produced by $^{13}\mathrm{C}(p, \alpha)^{10}\mathrm{B}$ after shock arrival. The amount of ^{10}B increases again in the expansion due to the supply, through the ν-process, of ^{12}C. A small amount of ^{10}B is also produced through $^{6}\mathrm{Li}(\alpha, \gamma)^{10}\mathrm{B}$ in the He/C layer. Destruction after shock passage is negligible in the He/C layer.

4.2. *Yields of Light Elements*

We consider light element yields resulting from different sets of the relevant ν-process cross sections. The yields of ^{7}Li, ^{11}B, ^{6}Li, ^{9}Be, ^{10}Be, and ^{10}B are listed in Table 10. We first compare the yields of the light elements of model 1 with those of model 1p (see § 3.2 and Table 9). In model 1 and model 2, new reaction rates obtained in § 2 with the WBP+SFO Hamiltonians and new branching ratios are used. Model 1p uses the reaction rates of ^{4}He and ^{12}C evaluated in SC06. The branching ratios used to produce ^{7}Li, ^{7}Be, ^{9}Be, and ^{10}B from ^{12}C were not evaluated in SC06. Therefore, we adopted the rates of these reactions from HW92 in model 1p (see also § 3.2).

The yields of ^{7}Li and ^{11}B in model 1 become slightly smaller than those in model 1p, but are not very different. ^{7}Li and ^{11}B are the main products of the ν-process from ^{4}He and ^{12}C. The cross

TABLE 10
YIELDS OF ^{7}Li, ^{11}B, ^{6}Li, ^{9}Be, ^{10}Be, AND ^{10}B

Species	Model 1 ($M_\odot$)	Model 1mk ($M_\odot$)	Model 2 ($M_\odot$)	Model 1p ($M_\odot$)	Model 1hw ($M_\odot$)
^{7}Li	2.67×10^{-7}	4.14×10^{-7}	2.54×10^{-7}	3.06×10^{-7}[a]	2.36×10^{-7}[b]
^{11}B	7.14×10^{-7}	8.67×10^{-7}	6.72×10^{-7}	7.51×10^{-7}[a]	6.26×10^{-7}[b]
^{6}Li	4.67×10^{-11}	3.60×10^{-11}	4.19×10^{-11}	4.61×10^{-12}	3.46×10^{-12}
^{9}Be	6.56×10^{-11}	9.65×10^{-11}	5.57×10^{-11}	1.69×10^{-11}	1.36×10^{-11}
^{10}Be	3.54×10^{-11}	3.55×10^{-11}	1.69×10^{-11}	4.18×10^{-12}	4.18×10^{-12}
^{10}B	1.08×10^{-9}	6.10×10^{-10}	1.05×10^{-9}	2.45×10^{-9}	2.45×10^{-9}

[a] Data are adopted from Table IV of Suzuki et al. (2006).
[b] Data are adopted from Yoshida et al. (2006b).

sections of ^{4}He$(\nu,\nu'p)^{3}$H and ^{4}He$(\nu,\nu'n)^{3}$He in this study are slightly smaller than those in SC06, owing to the consideration of the branches of *dd* and *nnpp*. The cross sections of ^{12}C$(\nu,\nu'x)^{11}$B and ^{12}C$(\nu,\nu'x)^{11}$C in this study scarcely change from those of SC06.

The ^{10}B yield of model 1 is smaller than that of model 1p by a factor of 2.3. This reflects the difference of the ν-process reaction rates to produce ^{10}B from ^{12}C. The total ν-process reaction rate to produce ^{10}B from ^{12}C in this study is smaller than that of HW92 by a factor of 3. The ^{10}B production through ^{6}Li$(\alpha,\gamma)^{10}$B in the He/C layer slightly suppresses the decrease.

The ^{9}Be yield in model 1 is larger than those in model 1p by a factor of 4. The neutrino reaction rate responsible for production of ^{9}Be in this study is larger than that used by HW92 by a factor of 6. Therefore, the enhancement of the ^{9}Be yield is not as large as that of the ν-process product ^{9}Be. The destruction of ^{9}Be during the explosion might suppress the yield enhancements.

The ^{6}Li yield in model 1 is larger than that in model 1p by about 1 order of magnitude. As explained in § 4.1.3, the new branches ^{4}He$(\nu,\nu'd)^{2}$H, ^{4}He$(\nu_e,e^{-}pp)^{2}$H, and ^{4}He$(\bar{\nu}_e,e^{+}nn)^{2}$H strongly enhance deuteron production. The produced deuterons are captured to produce ^{6}Li through ^{2}H$(\alpha,\gamma)^{6}$Li. This reaction sequence enhances the ^{6}Li yield by a factor of 5. The newly evaluated branches to produce ^{6}Li and the increasing reaction rate of ^{9}Be production through the ν-process from ^{12}C also enhance the ^{6}Li yield. Thus, it is important to evaluate the rates of the ν-process branches from ^{4}He and ^{12}C when the ^{6}Li yield is investigated.

We calculated the reaction cross sections of the ν-process branches to produce ^{10}Be. These reactions should enhance the yield of ^{10}Be. The yield of ^{10}Be in model 1 is larger than that in model 1p by a factor of 8.5. This is due to the additional ν-process reactions. We note that the yield of ^{10}Be strongly depends on the $\bar{\nu}_e$ temperature, because the cross section of ^{12}C$(\bar{\nu}_e,e^{+}x)^{10}$Be is large. In the case of model 2, which uses a $\bar{\nu}_e$ temperature smaller than that in model 1, the ^{10}Be yield is smaller than in model 1 by a factor of 2. This decrease is due to the decrease in the rate of ^{12}C$(\bar{\nu}_e,e^{+}x)^{10}$Be over that of model 1 by a factor of 5.

We compare ^{7}Li and ^{11}B yields of models 1 and 1hw (see Table 10). The ^{7}Li and ^{11}B yields of model 1 are larger by factors of 1.13 and 1.14 than the corresponding yields in model 1hw. The larger yields reflect the fact that the cross sections of neutrino-^{4}He reactions for neutral- and charged-current used in this study are larger than those of the corresponding values in HW92. On the other hand, the production of *n* and *p* through the ν-process might suppress the enhancement of the ^{7}Li and ^{11}B production. We note that the total cross section of neutral-current ν-process reactions on ^{12}C in this study is slightly smaller than that in HW92. However, the ^{11}B yield is not smaller than the one obtained with the old cross sections. Most of ^{11}B is produced through ^{7}Li$(\alpha,\gamma)^{11}$B and the ν-process from ^{12}C. The production through ^{7}Li$(\alpha,\gamma)^{11}$B increases the ^{11}B yield when the new reaction rates are used.

We also compare light-element yields of models 1 and 1mk. Model 1mk uses the same neutrino temperature set as model 1, and cross sections are evaluated using the PSDMK2 Hamiltonian for ^{12}C and SPSDMK for ^{4}He. The yield of ^{7}Li in model 1mk is larger than that in model 1 by a factor of 1.6. This is because the cross sections of ^{4}He with the SPSDMK Hamiltonian are larger than the corresponding ones with the WBP Hamiltonian for a given neutrino temperature. The yields of other light elements have dependencies similar to the cross sections of the ν-process reactions to produce the corresponding nuclei. In the case of ^{9}Be, the yield in model 1mk is larger than the corresponding yield in model 1. The ν-process production cross section exhibits the same trend. On the other hand, the yields of ^{6}Li and ^{10}B in model 1mk are smaller than those in model 1. The SPSDMK cross section of ^{4}He$(\nu,\nu'd)^{2}$H is smaller than the WBP one by more than a factor of 2. The PSDMK2 cross section to produce ^{10}B is also smaller than the one from the SFO Hamiltonian. The ^{10}Be yield is almost same between the two models. We do not find large differences in the cross section to produce ^{10}Be from ^{12}C in the neutrino temperature range in this study.

The case of ^{11}B is an exception. The yield of ^{11}B in model 1mk is larger than that in model 1 by a factor of 1.21, although the ν-process cross sections to produce ^{11}B and ^{11}C evaluated using PSDMK2 Hamiltonian are smaller than those using SFO. A large amount of ^{11}B is produced via ^{7}Li$(\alpha,\gamma)^{11}$B through the reaction sequence from ^{4}He$(\nu,\nu'p)^{3}$H$(\alpha,\gamma)^{7}$Li. The larger production of ^{11}B reflects the larger cross sections of ^{4}He$(\nu,\nu'p)^{3}$H evaluated using the SPSDMK Hamiltonian.

4.3. *Constraints on the Neutrino Energy Spectrum*

Light elements are continuously produced by Galactic cosmic rays (GCRs), nucleosynthesis in SNe, AGB stars, and so on. GCE models deduce the contributions of various production sites from the observed light-element abundances in stars as a function of their metallicity. The contribution of the ^{11}B yield in SNe was evaluated in GCE models (Fields et al. 2000; Ramaty et al. 2000a, 2000b; Alibés et al. 2002). The yield of ^{11}B in representative SNe of progenitor mass $\sim$20 $M_\odot$ is

$$3.3\times10^{-7}\ M_\odot \lesssim M\left(^{11}\mathrm{B}\right) \lesssim 7.4\times10^{-7}\ M_\odot. \quad (5)$$

Yoshida et al. (2005a) evaluated the range of the temperature of $\nu_{\mu,\tau}$ and $\bar{\nu}_{\mu,\tau}$ neutrinos, $T_{\nu_{\mu,\tau}}$, to be between 4.8 and 6.6 MeV. It was assumed that the energy spectra of SN neutrino follow Fermi-Dirac distributions with zero chemical potentials and

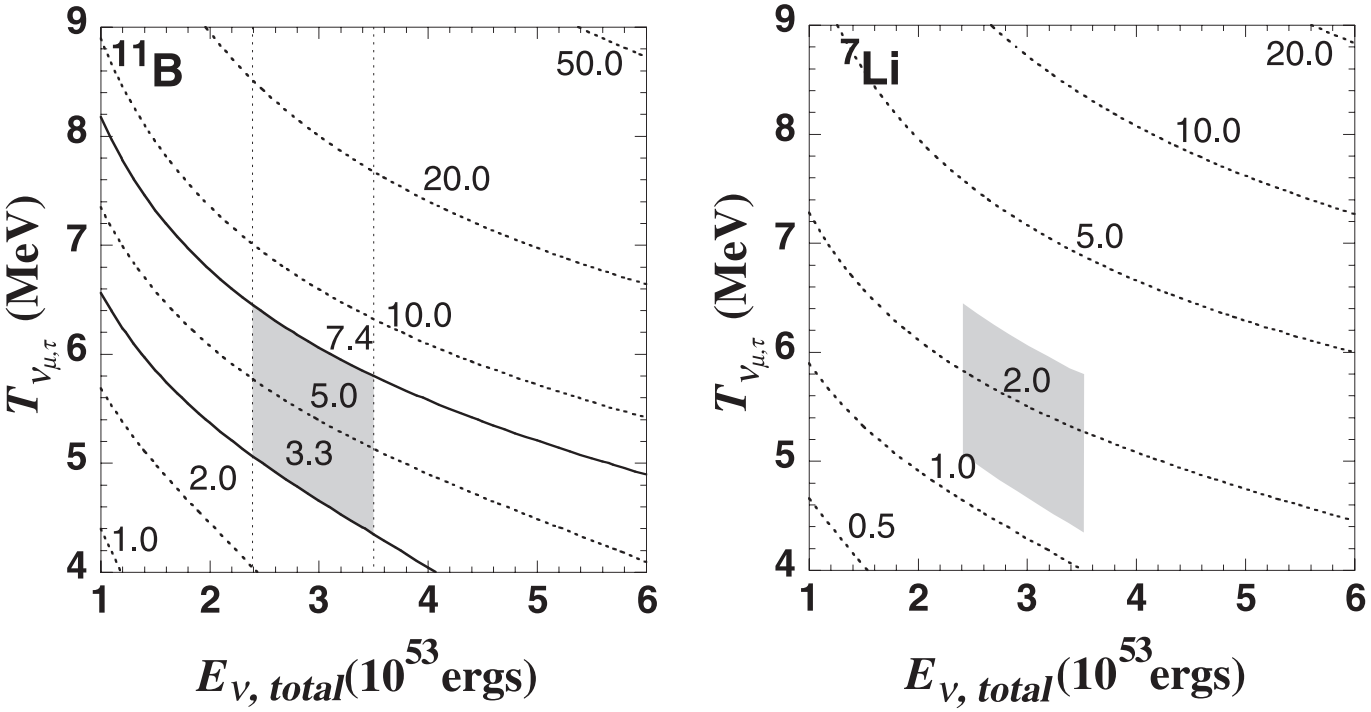

FIG. 5.—Contours of the yields of ^{11}B (*left*) and ^{7}Li (*right*) with SFO+WBP neutrino cross sections, as a function of total neutrino energy and the neutrino temperature $T_{\nu_{\mu,\tau}}$. The temperature of ν_e and $\bar{\nu}_e$ is assumed to be fixed at 4 MeV. The number attached to each line indicates the yield in units of $10^{-7}\,M_\odot$. The region between the two solid contour lines satisfies the SN contribution constraint from GCE modeling. The range between the two vertical dotted lines indicates the possible neutrino energy range evaluated for the gravitational energy of a neutron star. The shaded region satisfies both the ^{11}B GCE constraint and the total neutrino energy. [*See the electronic edition of the Journal for a color version of this figure.*]

$(T_{\nu_e}, T_{\bar{\nu}_e}) = (3.2\ \mathrm{MeV}, 5\ \mathrm{MeV})$. They also discussed the effects of the degeneracy of the neutrino energy spectra. However, the range of allowed neutrino temperatures also depends on the cross sections of the ν-process reactions. We reevaluate the range of neutrino temperatures from GCE model constraints with the new cross sections, and also discuss the yields of other light elements in the temperature range given by the ^{11}B constraint.

We calculated light-element nucleosynthesis in the $T_{\nu_{\mu,\tau}}$ range between 4 and 9 MeV on grids with steps of 0.2 MeV and in the E_ν range between 1×10^{53} and 6×10^{53} ergs on grids with steps of 1×10^{53} ergs. We fixed the temperatures of ν_e and $\bar{\nu}_e$ at 3.2 and 5 MeV, respectively, for simplicity, as in Yoshida et al. (2005a). Based on the nucleosynthesis calculations, we derive contours of ^{11}B yield in E_ν-$T_{\nu_{\mu,\tau}}$ space. Figure 5 shows the contours of the ^{11}B yield for the ν-process cross sections from the WBP+SFO model. The total neutrino energy deduced from the gravitational binding energy of a neutron star is in the range 2.4×10^{53} ergs $\le E_\nu \le 3.5\times10^{53}$ ergs. From the GCE range of the ^{11}B yield (SN component) and the above range for the total neutrino energy, we constrain the neutrino temperature to be confined in

$$4.3\ \mathrm{MeV} \lesssim T_{\nu_{\mu,\tau}} \lesssim 6.5\ \mathrm{MeV}. \quad (6)$$

This range is slightly smaller than the previously evaluated range; $4.8\ \mathrm{MeV} \lesssim T_{\nu_{\mu,\tau}} \lesssim 6.6\ \mathrm{MeV}$ (Yoshida et al. 2005a). The contours of the ^{7}Li yield are shown in Figure 5*b*. The yield expected from GCE considerations is indicated by the shaded region. We also evaluated the range of yields for other species, as allowed by the $T_{\nu_{\mu,\tau}}$ and $E_{\nu,\mathrm{total}}$ constraints (see Table 11). Yields of model 1 are in the allowed range for each nuclear species considered.

We note that the lower limit of $T_{\mu,\tau}$ is smaller than the assumed value of $T_{\bar{\nu}_e}$. If we assume that $T_{\nu_{\mu,\tau}}/T_{\bar{\nu}_e}$ keeps a constant ratio, the lower limit of $T_{\nu_{\mu,\tau}}$ should be larger. When we assume $T_{\nu_{\mu,\tau}}/T_{\bar{\nu}_e} = 1.2$, which is equal to the ratio in model 1, the lower limit of $T_{\nu_{\mu,\tau}}$ is 5.0 MeV. This corresponds to model ST (see Table 9).

TABLE 11
YIELD RANGES OF LIGHT ELEMENTS CONSTRAINED BY THE SN CONTRIBUTION OF ^{11}B IN GCE MODELS

	WBP+SFO MODEL		SPSDMK+PSDMK2 MODEL	
SPECIES	Minimum Yield ($M_\odot$)	Maximum Yield ($M_\odot$)	Minimum Yield ($M_\odot$)	Maximum Yield ($M_\odot$)
^{11}B	3.30×10^{-7}	7.40×10^{-7}	3.30×10^{-7}	7.40×10^{-7}
^{6}Li	2.21×10^{-11}	5.25×10^{-11}	1.39×10^{-11}	3.11×10^{-11}
^{7}Li	1.17×10^{-7}	2.82×10^{-7}	1.40×10^{-7}	3.37×10^{-7}
^{9}Be	2.94×10^{-11}	7.08×10^{-11}	3.23×10^{-11}	7.96×10^{-11}
^{10}Be	2.86×10^{-11}	3.94×10^{-11}	2.81×10^{-11}	3.96×10^{-11}
^{10}B	4.39×10^{-10}	1.20×10^{-9}	1.88×10^{-10}	5.30×10^{-10}

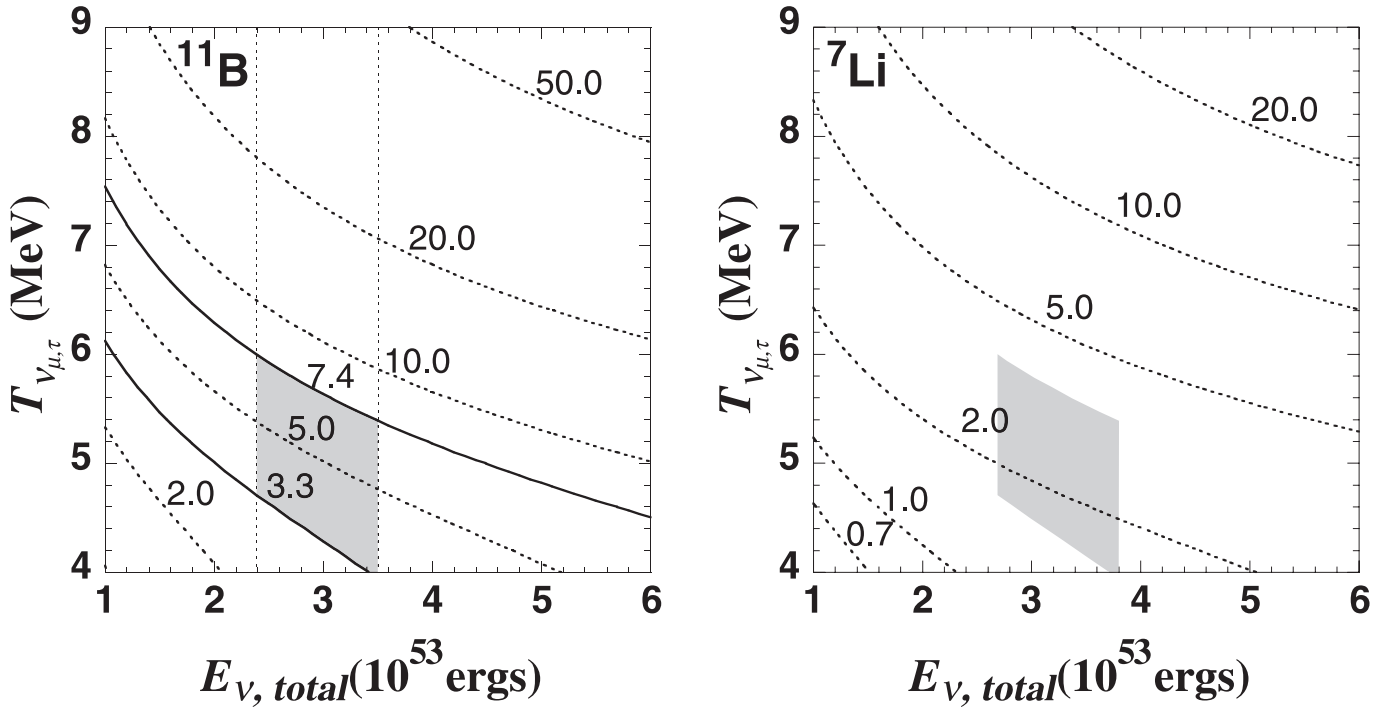

FIG. 6.—Same as Fig. 5, but for the SN model with PSDMK2+SPDMK-based neutrino cross sections. [*See the electronic edition of the Journal for a color version of this figure*.]

In order to exhibit the effects of different shell-model Hamiltonians, we evaluated the range of the neutrino temperature using the ν-process cross sections of the SPSDMK+PSDMK2 model. Figure 6*a* shows the corresponding contours of the ^{11}B yield for the SPSDMK+PSDMK2 model. With this cross section set, we find a larger yield of ^{11}B than for the WBP+SFO model, with the same neutrino radiation. The range of the neutrino temperature consistent with the ^{11}B constraint in GCE models is now

$$4.0\ \mathrm{MeV} \lesssim T_{\nu_{\mu,\tau}} \lesssim 6.0\ \mathrm{MeV}, \tag{7}$$

slightly shifted to smaller values than obtained in the WBP+SFO model.

Yields of other elements, constrained by the allowed ranges of neutrino temperature and total neutrino energy, are given in Table 11. The contours of the ^{7}Li yield are shown in Figure 6*b*. The upper and lower limits of the yields are different from those of the WBP+SFO model, but by less than 20% for most cases. This change is much smaller than the basic yield range for each species. However, the yields of ^{6}Li and ^{10}B show relatively large differences, due to the difference of the contribution from $^{4}\mathrm{He}(\nu, \nu' d)^{2}\mathrm{H}$.

4.4. *Effect of Neutrino Chemical Potential*

Most of the calculations on the ν-process in supernovae are performed with the neutrino energy spectra, assuming Fermi-Dirac distributions and zero chemical potentials. On the other hand, studies of detailed neutrino transport in core-collapse supernovae have shown that the neutrino energy spectra are closer to a slightly "degenerate" distribution than those with zero chemical potential. In order to investigate the detailed dependence on neutrino degeneracy, the ν-process cross sections as a function of the neutrino energy are required. Here we investigate the effects of the neutrino degeneracy on the light-element yields. We note that we take into account the neutrino degeneracy only for the ν-process of ^{4}He and ^{12}C. We do not take into account the neutrino degeneracy for other ν-process reactions adopted from HW92, because their reaction rates are shown with definite neutrino temperatures derived with the assumption of Fermi-Dirac distributions with zero chemical potential.

The yield ratios of ^{7}Li and ^{11}B relating to the neutrino degeneracy parameter $\eta_\nu = \mu_\nu / kT_\nu$ are shown in Figure 7. Here we assumed that the degeneracy parameter η_ν does not depend on neutrino flavors. The yield ratios increase with the neutrino degeneracy. In the case of $\eta_\nu = 3$, the yield ratios of ^{7}Li and ^{11}B are 1.4 and 1.5, respectively. Yoshida et al. (2005a) discussed the

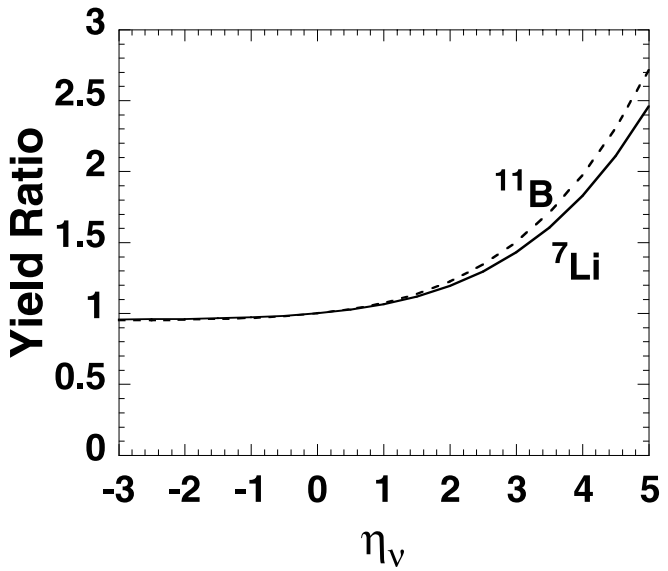

FIG. 7.—Relation between the yield ratios of ^{7}Li (*solid lines*) and ^{11}B (*dotted lines*) to those in case of model 1 and the neutrino degeneracy parameter η_ν. The neutrino temperatures and the total neutrino energy are fixed to the values of $(T_{\nu_e}, T_{\bar{\nu}_e}, T_{\nu_{\mu,\tau}}, E_{\nu,\mathrm{total}}) = (3.2\ \mathrm{MeV}, 5\ \mathrm{MeV}, 6\ \mathrm{MeV}, 3 \times 10^{53}\ \mathrm{ergs})$.

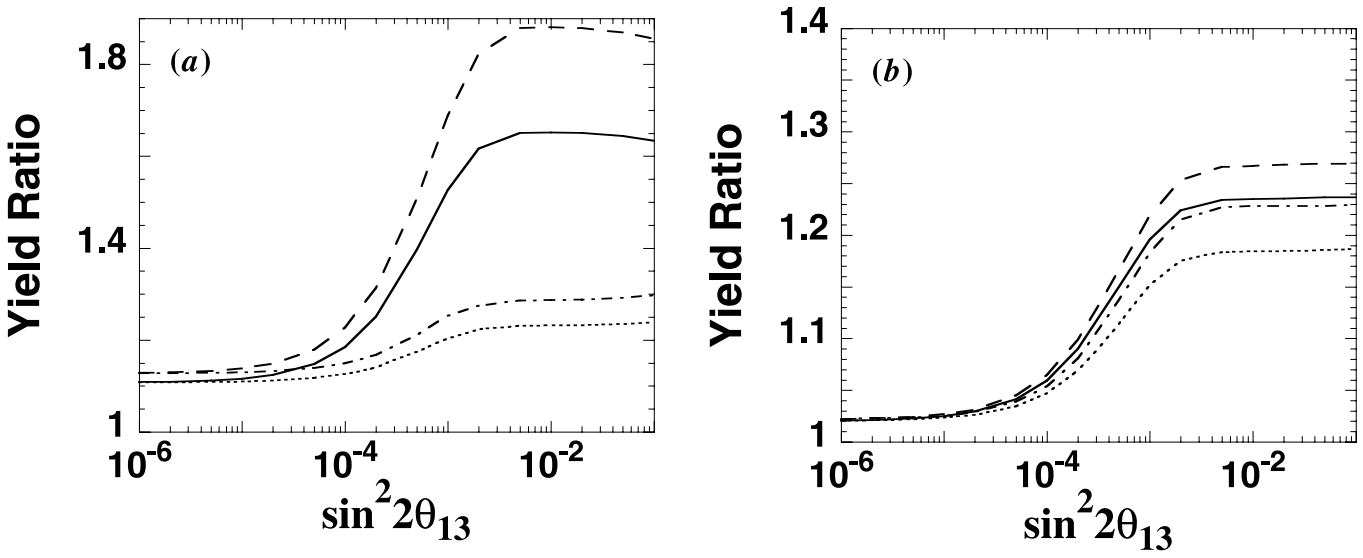

FIG. 8.—Yield ratios of (*a*) ^{7}Li and (*b*) ^{11}B. Solid and dotted lines correspond to normal and inverted mass hierarchies, respectively, in model 1. Dashed and dot-dashed lines correspond to normal and inverted mass hierarchies in model 1hw.

effect of the neutrino degeneracy on the light-element yields using an analytical approximation for the ν-process cross sections of ^{4}He and ^{12}C. We find that the ^{7}Li and ^{11}B yields in the case of $\eta_\nu = 3$ would be increased by about 50% compared to the yields for $\eta_\nu = 0$. Therefore, our analytical evaluation approximates the numerical evaluation well. We obtained a similar dependence of the yield ratios on the neutrino degeneracy for the other light elements; the yield ratios are between 1.4 and 1.5 in the case of $\eta_\nu = 3$. The constraint of the neutrino temperature is smaller by about 0.1 MeV in the case of $\eta_\nu = 3$ (Yoshida et al. 2005a).

5. CHANGED ^{7}Li AND ^{11}B YIELDS DUE TO NEUTRINO OSCILLATIONS

Neutrino oscillations change the flavors of the neutrinos emitted from the neutrino sphere during their passage through the stellar interior. The average neutrino energies of ν_e and $\bar{\nu}_e$ increase due to the neutrino oscillations, and their enhancement depends on neutrino oscillation parameters, i.e., mass hierarchy and the mixing angle θ_{13}. In this study, we evaluate the flavor transition probabilities by the neutrino oscillations using the same procedure as in Yoshida et al. (2006a, 2006b). We evaluate the rates of the charged-current ν-process reactions of ^{4}He and ^{12}C using the flavor-transition probabilities and the cross sections derived in § 2. Then we calculate detailed nucleosynthesis with the ν-process reactions.

5.1. *Differences Due to New Neutrino-Nucleus Cross Sections*

The dependence of the ^{7}Li and ^{11}B yields on neutrino oscillation parameters is influenced by the cross sections of neutrino-nucleus reactions (Yoshida et al. 2006a, 2006b). We study the effects on the ^{7}Li and ^{11}B yields due to neutrino oscillations by comparing models 1 and 1hw. Model 1hw is the standard model in Yoshida et al. (2006a, 2006b).

Figure 8*a* shows the relation between the ^{7}Li yield ratio, i.e., the ratio of the ^{7}Li yield to the one without neutrino oscillations, and the mixing angle $\sin^2 2\theta_{13}$. We observe that the dependence on the oscillation parameters, i.e., mass hierarchies and mixing angle θ_{13}, does not change qualitatively. The increase in the ^{7}Li yield is larger in a normal mass hierarchy than in an inverted hierarchy, and the yield increases for the case of $\sin^2 2\theta_{13} \gtrsim 2 \times 10^{-3}$, i.e., the H resonance is adiabatic. On the other hand, the maximum value of the yield ratio is somewhat reduced. The maximum yield ratio is 1.65, which is smaller than the value of 1.87 found in the previous study. The maximum ^{7}Li yield is $4.41 \times 10^{-7}\ M_\odot$ in a normal mass hierarchy and for $\sin^2 2\theta_{13} = 1 \times 10^{-2}$. The difference of the neutral-current cross section of ^{4}He becomes larger for a smaller neutrino temperature. In this case, the contribution from the neutral-current reactions of ν_e and $\bar{\nu}_e$ is larger in the new rates than it is for the HW92 rates. The contribution from charged-current reactions in the new rates becomes smaller.

In the case of an inverted mass hierarchy, the maximum increase in the ^{7}Li yield is a factor of 1.24, which is slightly smaller than the value found in the previous study. The new reaction rates slightly decrease the effect of neutrino oscillations. The maximum yield of ^{7}Li is $3.31 \times 10^{-7}\ M_\odot$ for $\sin^2 2\theta_{13} = 0.1$.

Figure 8*b* shows the dependence of the ^{11}B yield ratio on the mixing angle $\sin^2 2\theta_{13}$ using the new and old cross sections. The ^{11}B yield increases most effectively in a normal mass hierarchy and for the case of the adiabatic H resonance. The ^{11}B yield reaches $8.83 \times 10^{-7}\ M_\odot$ in the case of a normal mass hierarchy and $\sin^2 2\theta_{13} = 0.1$. The maximum yield ratio is 1.24. The maximum increase in the ^{11}B yield is smaller with the new cross sections. In the case of an inverted mass hierarchy, the increase in the ^{11}B yield is smaller than the corresponding value in a normal mass hierarchy. The maximum yield is $8.48 \times 10^{-7}\ M_\odot$ for $\sin^2 2\theta_{13} = 0.1$. The maximum yield ratio is 1.19.

5.2. *Dependence on $T_{\nu_{\mu,\tau}}$*

We investigated the dependence of the ^{11}B yield on the temperature of $\nu_{\mu,\tau}$ and $\bar{\nu}_{\mu,\tau}$ neutrinos, and evaluated the temperature range satisfying the ^{11}B abundance constraints in GCE models (Yoshida et al. 2005a). This range also depends on the cross sections of the ν-process. Therefore, we consider models LT and ST, which present $T_{\nu_{\mu,\tau}}$ and E_ν values different from model 1 (see § 3.2). The values of the neutrino temperatures and the total neutrino energy are given in Table 9.

When neutrino oscillations are not considered, the ^{7}Li yield varies between 1.39×10^{-7} and $2.88 \times 10^{-7}\ M_\odot$ due to the allowed range of the neutrino temperature $T_{\nu_{\mu,\tau}}$. The variation of the ^{11}B yield is between 3.56×10^{-7} and $7.46 \times 10^{-7}\ M_\odot$. Both

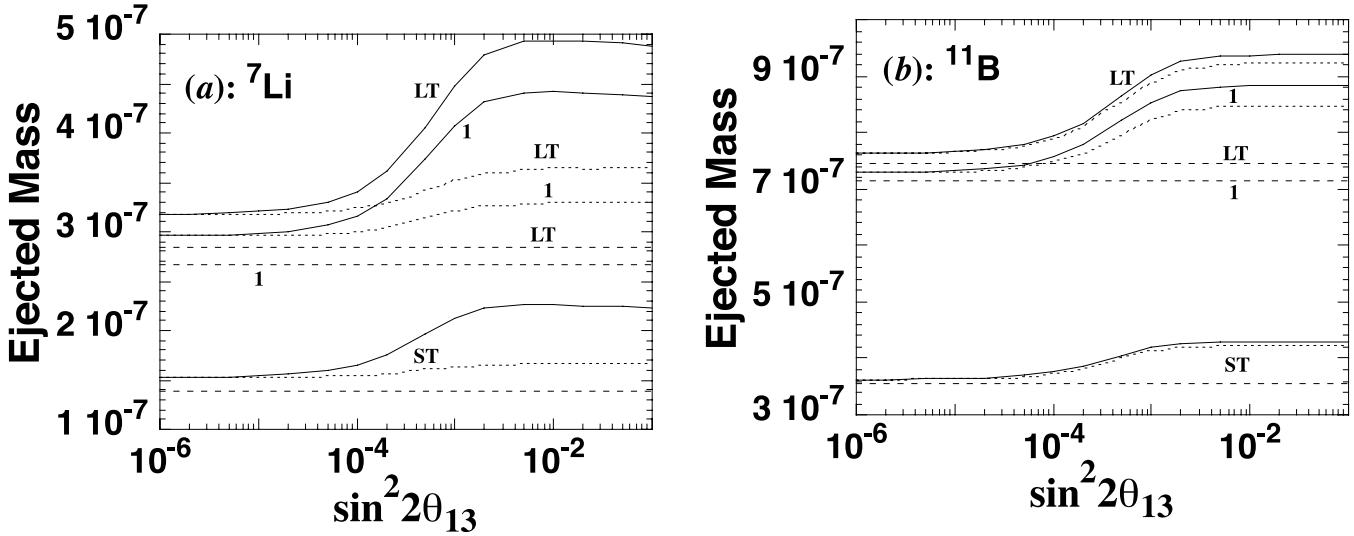

FIG. 9.—Dependence of the yields of (*a*) ^{7}Li and (*b*) ^{11}B in units of $M_{\odot}$ on mixing angle $\sin^2 2\theta_{13}$ with different assumptions for the neutrino temperature $T_{\nu_{\mu,\tau}}$. Black, blue, and red lines indicate models, 1, ST, and LT, respectively. Solid and dotted lines correspond to the normal and inverted mass hierarchies, respectively. [*See the electronic edition of the Journal for a color version of this figure.*]

yields thus change by about a factor of 2 over this temperature range. Therefore, we must consider variations due to neutrino oscillations as well as neutrino temperature.

The dependence of the ^{7}Li and ^{11}B yields on mass hierarchies and the mixing angle θ_{13} in these three models is shown in Figure 9. We observe that the ^{7}Li yield varies between 1.39×10^{-7} and 4.93×10^{-7} $M_{\odot}$, widening with increasing temperature. However, it is difficult to distinguish the effect of neutrino oscillations and temperature. If the ^{7}Li yield is smaller than 3.2×10^{-7} $M_{\odot}$, the increase in the yield due to the neutrino oscillations cannot be distinguished from the ^{7}Li yield range deduced from the uncertainty of the neutrino temperature. Even for a larger ^{7}Li yield, the constraints on the mass hierarchy and the mixing angle θ_{13} become ambiguous due to the uncertainty in the neutrino temperature.

Figure 9*b* shows that the variation of the ^{11}B yield is between 3.56×10^{-7} and 9.40×10^{-7} $M_{\odot}$. However, as pointed out above, it is difficult to constrain oscillation parameters. If the ^{11}B yield is smaller than 7.6×10^{-7} $M_{\odot}$, the uncertainty due to the neutrino temperature and the increase in the yield due to neutrino oscillations are not distinguishable. Even for larger yields, there are no clear differences between the yields in a normal mass hierarchy and in an inverted mass hierarchy.

5.3. *Constraints on Oscillation Parameters from the* ^{7}Li/^{11}B *Ratio*

In Yoshida et al. (2006a, 2006b) we proposed a constraint of neutrino oscillation parameters derived from the ^{7}Li/^{11}B abundance ratio. We have shown above that both the ^{7}Li and ^{11}B yields change with the neutrino temperature by about a factor of 2. When the abundance ratio of ^{7}Li/^{11}B is considered, the uncertainty due to the neutrino temperature cancels out. Then, the dependence on mass hierarchy and mixing angle θ_{13} is most clearly revealed. We found that the ^{7}Li/^{11}B ratio is larger than 0.83 in a normal mass hierarchy and $\sin^2 2\theta_{13} \gtrsim 2 \times 10^{-3}$. When we do not consider neutrino oscillations, the ^{7}Li/^{11}B ratio is 0.71, at most. However, the ^{7}Li/^{11}B ratio does depend on the relevant ν-process cross sections. We evaluate the range of the ^{7}Li/^{11}B ratio with the new cross sections discussed in § 2.

We evaluate the ^{7}Li/^{11}B range using models 1, 2, LT, and ST. Figure 10 shows the abundance ratio of ^{7}Li/^{11}B with the relation to $\sin^2 2\theta_{13}$ evaluated using the WBP+SFO model. When we do not consider neutrino oscillations, the ^{7}Li/^{11}B ratio lies between 0.59 and 0.61. The ^{7}Li/^{11}B ratio changes by about 12% among these four neutrino temperature models. As shown in Yoshida et al. (2006a, 2006b), the uncertainties of the ^{7}Li and ^{11}B yields by neutrino temperatures are canceled out when we adopt the ^{7}Li/^{11}B ratio.

In a normal mass hierarchy, the ^{7}Li/^{11}B ratio depends on $\sin^2 2\theta_{13}$. For the nonadiabatic H resonance, the ^{7}Li/^{11}B ratio lies between 0.64 and 0.66; the range is slightly larger than the case without neutrino oscillations. This slight increase is due to the fact that the ^{7}Li yield is larger even in nonadiabatic H resonance. For an adiabatic H resonance, where $\sin^2 2\theta_{13} \geq 0.002$, the ^{7}Li/^{11}B ratio is in the range of 0.78–0.83. The increase is slightly smaller than the one found in Yoshida et al. (2006a). The value of 0.78 corresponds to model 1. As discussed in Yoshida et al. (2006b),

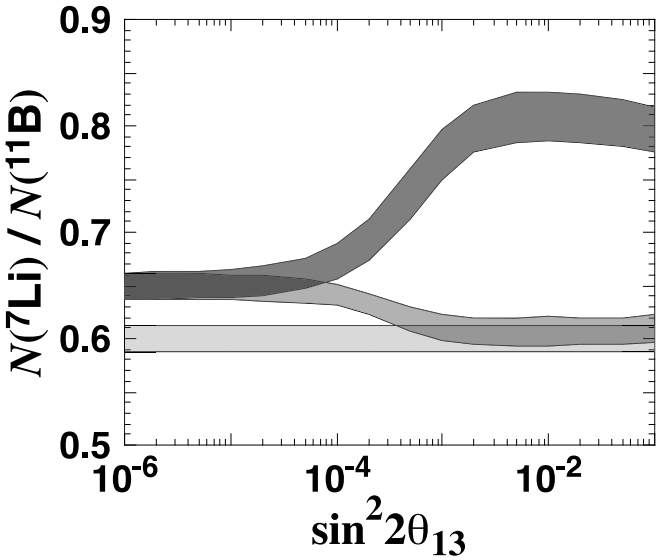

FIG. 10.—^{7}Li/^{11}B abundance ratio as a function of the mixing angle $\sin^2 2\theta_{13}$. Dark and medium shaded regions correspond to normal and inverted mass hierarchies, respectively. The lightly shaded region indicates the ratio obtained without neutrino oscillations. Each range is drawn using the results of models 1, 2, LT, and ST.

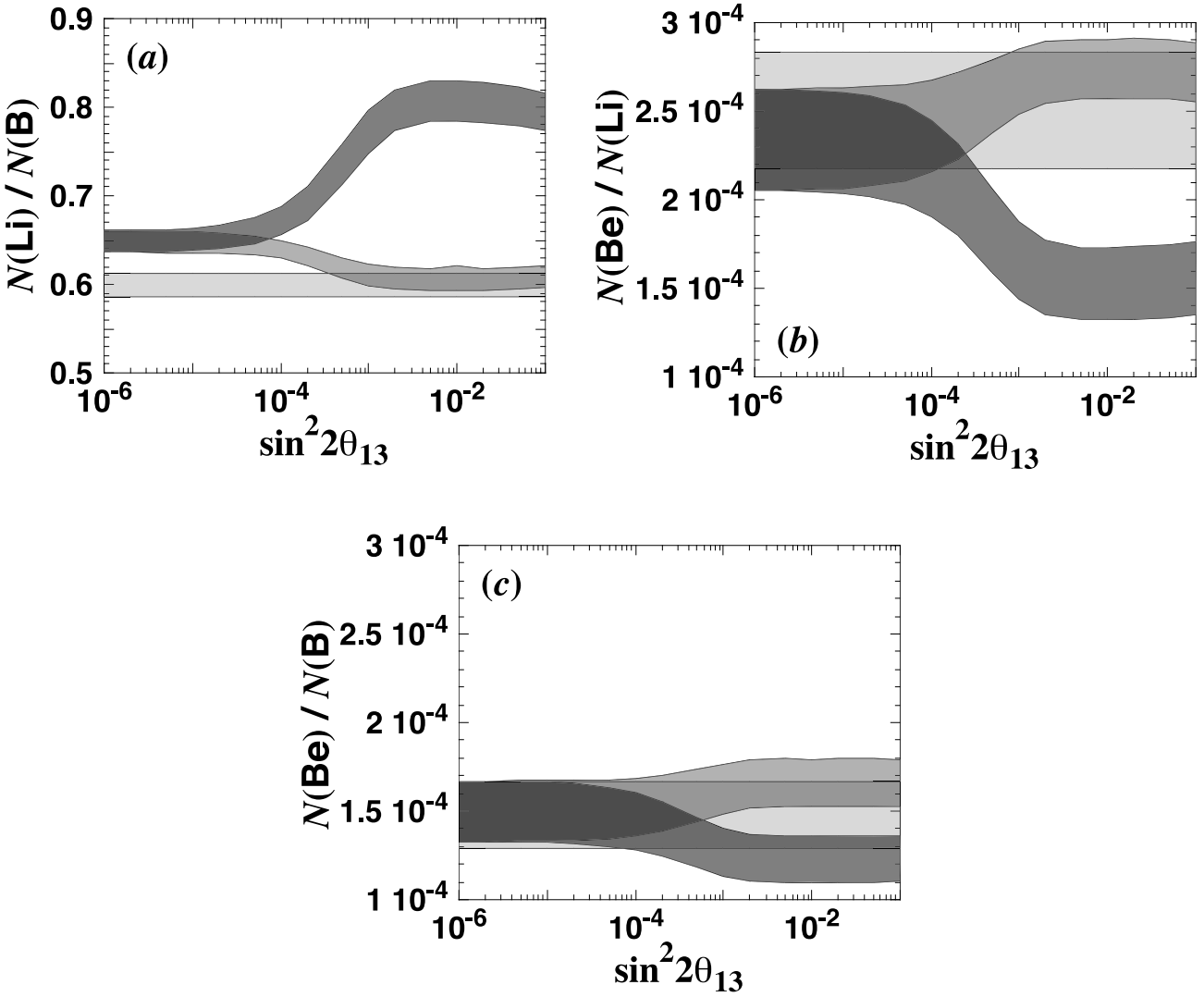

FIG. 11.—Elemental abundance ratios of (*a*) Li/B, (*b*) Be/Li, and (*c*) Be/B as a function of the mixing angle $\sin^2 2\theta_{13}$. Dark and medium shaded regions correspond to normal and inverted mass hierarchies, respectively. The lightly shaded region indicates the ratio obtained without neutrino oscillations. Each range is drawn using the results of models 1, 2, LT, and ST.

the variation of the ^{7}Li/^{11}B ratio for a given value of $\sin^2 2\theta_{13}$ is mainly due to the uncertainties of T_{ν_e} and $T_{\bar{\nu}_e}$. If the uncertainty of T_{ν_e} and $T_{\bar{\nu}_e}$ becomes small, the range of ^{7}Li/^{11}B in adiabatic resonance becomes small.

In an inverted mass hierarchy, the ^{7}Li/^{11}B ratio is not distinguishable from the one with normal mass hierarchy or without neutrino oscillations. If the H resonance is nonadiabatic, the ^{7}Li/^{11}B ratio is identical in normal and inverted mass hierarchies. The ^{7}Li/^{11}B ratio for an adiabatic H resonance is smaller than the one for a nonadiabatic resonance.

For completeness, we also show the elemental abundance ratios of light elements in Figure 11. The Li/B ratio is almost identical to the ^{7}Li/^{11}B ratio. This is because most of Li and B are produced as ^{7}Li and ^{11}B, respectively. The Be/Li and Be/B ratios are much smaller than the Li/B ratio because the Be yield is much smaller than those of Li and B. The Be/Li ratio shows a dependence on mass hierarchies in the case of $\sin^2 2\theta_{13} \gtrsim 2 \times 10^{-3}$. The Be/Li ratio is smaller than 1.8×10^{-4} in a normal mass hierarchy. On the other hand, it is larger than 2.1×10^{-4} in an inverted mass hierarchy. While the ^{7}Li abundance increases, the ^{9}Be abundance becomes slightly smaller, due to the destructive reaction $^9\mathrm{Be}(p, \alpha)^6\mathrm{Li}$. The contribution of $^{12}\mathrm{C}(\nu_e, e^- x)^9\mathrm{Be}$ does not affect the ^{9}Be yield, because the cross section is very small, even with the enhancement of the average ν_e energy (see Figs. 2 and 3).

The Be/B ratio has a small dependence on mass hierarchies and mixing angle θ_{13}. The variation of the ratio due to these parameters is roughly equal to the uncertainty resulting from the neutrino temperatures. From the viewpoint of elemental abundance ratios, the Li/B and Be/Li ratios depend on mass hierarchies and the mixing angle θ_{13}.

We have shown above that the ^{7}Li/^{11}B ratio in a normal mass hierarchy and adiabatic H resonance ($\sin^2 2\theta_{13} \gtrsim 2 \times 10^{-3}$) is larger than the one obtained in the other cases. This increase is attributed to the effect of neutrino oscillations, and remains after taking into account uncertainties in neutrino energy spectra. Therefore, we confirm with the new ν-process cross sections that the ^{7}Li/^{11}B ratio is a promising probe of oscillation parameters. If we find that the yields of ^{7}Li and ^{11}B produced in supernovae require a ^{7}Li/^{11}B ratio larger than 0.78, the mass hierarchy should be normal, and $\sin^2 2\theta_{13}$ should be larger than 2×10^{-3}. We expect that ^{7}Li and ^{11}B will eventually be detected in stellar material, indicating traces of SN material. Supernova remnants are also promising candidates

for this type of abundance constraint on neutrino physics. There have been attempts to find stars with excesses in ^{11}B, which would provide evidence for direct pollution with supernova ejecta (e.g., Rebull et al. 1998; Primas et al. 1998, 1999). The ^{7}Li/^{11}B ratio of presolar grains from SNe might also provide useful information (for presolar grains, see, e.g., Lodders & Amari 2005). On the other hand, there are still theoretical uncertainties regarding neutrino energy spectra and stellar evolution. The reduction of these uncertainties will bring about a stronger constraint on neutrino oscillation parameters.

The observation of supernova neutrino signals just after a supernova explosion is one of the most promising methods to constrain unknown neutrino oscillation parameters. It is expected that SuperKamiokande will detect more than 1000 neutrinos if a supernova explodes at the Galactic center (e.g., Fogli et al. 2005). If detailed energy spectra of the neutrinos emitted from the supernova are theoretically predicted, the analysis of the observed neutrino spectra will constrain the oscillation parameters (e.g., Dighe & Smirnov 2000; Takahashi et al. 2001). The time evolution of the neutrino signal may reveal the change of the neutrino spectra due to the supernova shock propagation (Takahashi et al. 2003; Tomàs et al. 2004; Fogli et al. 2005; Kneller et al. 2008). SuperKamiokande detects electron-type antineutrinos, so that the enhancement of the supernova $\bar{\nu}_e$ signal detected by SuperKamiokande will be evidence for an inverted mass hierarchy and relatively large value of θ_{13} ($\sin^2 2\theta_{13} \gtrsim 10^{-3}$). The enhancement of the ^{7}Li/^{11}B ratio will be evidence for a normal mass hierarchy and relatively large value of θ_{13}. Therefore, these two constraints complement each other.

6. DISCUSSION

6.1. *Temperatures of the ν_e and $\bar{\nu}_e$ Neutrinos*

The temperatures of the ν_e and $\bar{\nu}_e$ neutrinos are less sensitive to the yield constraints than those of the $\nu_{\mu,\tau}$ and $\bar{\nu}_{\mu,\tau}$, $T_{\nu_{\mu,\tau}}$ neutrinos. The temperatures T_{ν_e} and $T_{\bar{\nu}_e}$ are smaller than $T_{\nu_{\mu,\tau}}$ if neutrino oscillations are not taken into account. On the other hand, the enhancement of the light-element yields by neutrino oscillations do depend on T_{ν_e} and $T_{\bar{\nu}_e}$. The production through charged-current reactions is more enhanced when the temperature difference of ν_e and $\nu_{\mu,\tau}$ or $\bar{\nu}_e$ and $\nu_{\mu,\tau}$ is larger. Yoshida et al. (2006b) showed that the ^{7}Li/^{11}B ratio exhibits significant variation from different values of T_{ν_e} and $T_{\bar{\nu}_e}$ even for a fixed value of T_{ν}.

Yields of species mainly produced through charged-current ν-process reactions can be used to constrain the temperatures T_{ν_e} and $T_{\bar{\nu}_e}$. Isotopes of special importance are ^{138}La and ^{180}Ta (Goriely et al. 2001; Rauscher et al. 2002; Heger et al. 2005). The main production process of ^{138}La and ^{180}Ta is ^{138}Ba$(\nu_e, e^-)^{138}$La and ^{180}Hf$(\nu_e, e^-)^{180}$Ta, respectively. For ^{180}Ta, about half of the yield is produced through ^{181}Ta$(\gamma, n)^{180}$Ta and ^{181}Ta$(\nu, \nu' n)^{180}$Ta. The GT strength distributions in ^{138}La and ^{180}Ta were recently obtained experimentally (Byelikov et al. 2007). If the temperature of ν_e could be constrained from the yields of ^{138}La and ^{180}Ta and their observed abundances, the effect of neutrino oscillations on ν-process nucleosynthesis could be evaluated more precisely.

6.2. *Uncertainties in the Rates of ^{7}Li and ^{11}B Production Reactions*

In the He/C layer, almost all ^{7}Li are produced through ^{3}H$(\alpha, \gamma)^{7}$Li and ^{3}He$(\alpha, \gamma)^{7}$Be after the production of ^{3}H and ^{3}He through the ν-process. About 60% of ^{11}B is also produced through ^{7}Li$(\alpha, \gamma)^{11}$B in the inner region of the He/C layer. Therefore, the uncertainty of the rates of these reactions affects the yields of ^{7}Li and ^{11}B. We discuss this uncertainty briefly.

We adopted the rates of the three reactions from NACRE compilation (Angulo et al. 1998). The rates of ^{3}H$(\alpha, \gamma)^{7}$Li and ^{3}He$(\alpha, \gamma)^{7}$Be are in very good agreement with those in Caughlan & Fowler (1988). For ^{7}Li$(\alpha, \gamma)^{11}$B, the NACRE compilation showed slightly larger rate ($\sim$20% in the temperature range between 2×10^8 and 4×10^9 K) than in Caughlan & Fowler (1988). The NACRE compilation also showed uncertainties of their reaction rates; these are 11%, 17%, and 16% for ^{3}H$(\alpha, \gamma)^{7}$Li, ^{3}He$(\alpha, \gamma)^{7}$Be, and ^{7}Li$(\alpha, \gamma)^{11}$B, respectively. Therefore, the ^{7}Li and ^{11}B yields would have the uncertainty of about 17% due to the uncertainty of the reaction rates. The uncertainty of the ^{7}Li/^{11}B ratio would be smaller, because more than half of the ^{11}B is produced through the common production sequence of ^{7}Li in the He/C layer.

6.3. *Neutrino-Neutrino Interactions*

It has been pointed out that neutrino-neutrino interactions in regions just above a proto–neutron star change neutrino flavors and thus affect the neutrino energy spectra. These interactions contribute diagonal and off-diagonal potential to the flavor-basis Hamiltonians. This potential plays a complicated role in flavor exchange, due to the momentum transfer by the interactions. Analytical evaluation have been carried out in some special cases (e.g., Qian & Fuller 1995; Pastor & Raffelt 2002; Fuller & Qian 2006). The change of the neutrino energy spectra for two neutrino flavors by neutrino-neutrino interactions has been investigated in neutrino-driven winds (e.g., Duan et al. 2006a, 2006b) and in the density profile of an exploding supernova (e.g., Fogli et al. 2007). The neutrino-neutrino interactions in three neutrino flavors have very recently been investigated (Duan et al. 2008a, 2008b; Esteban-Pretel et al. 2008). It has been proposed that these interactions affect the efficiency of *r*-process nucleosynthesis (Balantekin & Yüksel 2005).

Neutrino-neutrino interactions may also change the locations of resonance to deeper regions, which could affect the ^{7}Li and ^{11}B yields in supernovae.

7. CONCLUSIONS

We evaluated the neutrino-nucleus reaction cross sections for ^{4}He and ^{12}C using new shell-model Hamiltonians. These cross sections are important for the yields of the light elements Li, Be, and B produced through the ν-process in SNe. We investigated the nucleosynthesis of the light elements in a SN model corresponding to SN 1987A using these new cross sections. We investigated the dependence of the light element yields on cross sections, neutrino energy spectra, and neutrino oscillations. We obtained the following results.

1. The neutrino-nucleus reaction cross sections are evaluated using WBP and SPSDMK Hamiltonians for ^{4}He and SFO and PSDMK2 Hamiltonians for ^{12}C. Main production channels of the ^{12}C reaction are the nuclei n, p, ^{4}He, ^{11}B, and ^{11}C. Production of ^{6}Li, ^{9}Be, ^{10}Be, and ^{10}B is also important.

2. For a given neutrino temperature set, the yields of ^{7}Li and ^{11}B with the cross sections of WBP+SFO model are larger than those of the cross sections in Woosley et al. (1990). This is mainly due to larger cross sections of ^{4}He$(\nu, \nu' p)^{3}$H and ^{4}He$(\nu, \nu' n)^{3}$He.

3. Larger yields of ^{6}Li and ^{9}Be result from the new cross sections, with the exception of the yield of ^{10}B, which is reduced. These changes reflect the difference of the cross sections of the ν-process for ^{12}C and deuteron production branches of ^{4}He. Radioactive ^{10}Be is produced with abundance levels similar to ^{6}Li. The channel for producing ^{6}Li and ^{10}Be have been evaluated in the ν-process of ^{12}C.

4. The larger cross sections slightly decrease the range of acceptable neutrino temperature, as constrained by the ^{11}B abundance evolution during GCE. The range of the neutrino temperature is 4.3 MeV $\lesssim T_{\nu_{\mu,\tau}} \lesssim$ 6.5 MeV for WBP+SFO model and 4.0 MeV $\lesssim T_{\nu_{\mu,\tau}} \lesssim$ 6.0 MeV for the SPSDMK+PSDMK2 model.

5. The dependence of the ^{7}Li and ^{11}B yields on neutrino oscillation parameters, such as mass hierarchy and the mixing angle θ_{13}, is not changed by the new cross sections. Yield enhancements are smaller.

6. The ^{7}Li/^{11}B abundance ratio depends on mass hierarchy and the mixing angle θ_{13}, even when considering uncertainties of neutrino temperatures and the total neutrino energy. For a normal mass hierarchy and $\sin^2 2\theta_{13} \gtrsim 2 \times 10^{-3}$, i.e., adiabatic H resonance, the ^{7}Li/^{11}B ratio is larger than 0.78. In the case of an inverted mass hierarchy or the case without neutrino oscillations, the ^{7}Li/^{11}B ratio is smaller than 0.61. Smaller uncertainty of neutrino temperatures extends the difference in the ^{7}Li/^{11}B ratio.

7. The Be/Li abundance ratio is very small. A decrease in the Be/Li ratio is seen for a normal mass hierarchy and $\sin^2 2\theta_{13} \gtrsim 2 \times 10^{-3}$.

We would like to thank Koichi Iwamoto, Ken'ichi Nomoto, and Toshikazu Shigeyama for providing the data for the internal structure of progenitor model 14E1 and for helpful discussions. Numerical computations were in part carried out on general common-use computer system at Center for Computational Astrophysics, CfCA, of National Astronomical Observatory of Japan. This work has been supported in part by the Ministry of Education, Culture, Sports, Science and Technology, Grants-in-Aid for Young Scientist (B) (17740130) and Scientific Research (C) (17540275, 18540290, 18560805), Mitsubishi Foundation, and the JSPS Core-to-Core Program, International Research Network for Exotic Femto Systems (EFES).

REFERENCES

Ahmed, S. N., et al. 2004, Phys. Rev. Lett., 92, 181301
Ahrens, J, et al. 1975, Nucl. Phys. A, 251, 479
Alibés, A., Labay, J., & Canal, R. 2002, ApJ, 571, 326
Angulo, C et al. 1998, Nucl. Phys. A, 656, 3
Apollonio, M., et al. 2003, European Phys. J. C, 27, 331
Araki, T., et al. 2005, Phys. Rev. Lett., 94, 081801
Ashie, Y., et al. 2004, Phys. Rev. Lett., 93, 101801
Balantekin, A. B., & Yüksel, H. 2005, New J. Phys., 7, 51
Brown, B., Etchegoyen, A., & Rae, W. D. M. 1986, OXBASH, the Oxford, Buenos-Aires, Michigan State Shell Model Program (MSU Cyclotron Laboratory Rept. 524; East Lansing: MSU)
Byelikov, A., et al. 2007, Phys. Rev. Lett., 98, 082501
Caughlan, G. A., & Fowler, W. A. 1988, At. Data Nucl. Data Tables, 40, 283
Colella, P., & Woodward, P. R. 1984, J. Comput. Phys., 54, 174
Dighe, A. S., & Smirnov, A. Y. 2000, Phys. Rev. D, 62, 033007
Domogatsky, G. V., Eramzhyan, R. A., & Nadyozhin, D. K. 1978, in Proc. Int. Conf. on Neutrino Physics and Neutrino Astrophysics, ed. M. A. Markov, G. V. Domogatsky, A. A. Komar, & A. N. Tavkhelidze (Moscow: Nauka), 115
Drake, T. E., Tomusiak, E. L., & Caplan, H. S. 1968, Nucl. Phys. A, 118, 138
Duan, H., Fuller, G. M., Carlson, J., & Qian, Y.-Z. 2006a, Phys. Rev. Lett., 97, 241101
———. 2006b, Phys. Rev. D, 74, 105014
———. 2008a, Phys. Rev. Lett., 100, 021101
———. 2008b, Phys. Rev. D, 77, 085016
Esteban-Pretel, A., Pastor, S., Tomás, R., & Raffelt, G. G. 2008, Phys. Rev. D, 77, 065024
Fields, B. D., Olive, K. A., Vangioni-Flam, E., & Cassé, M. 2000, ApJ, 540, 930
Fogli, G. L., Lisi, E., Marrone, A., & Mirizzi, A. 2007, J. Cosmol. Astropart. Phys., 12, 010
Fogli, G. L., Lisi, E., Mirizzi, A., & Montatino, D. 2005, J. Cosmol. Astropart. Phys., 04, 002
Fuller, G. M., & Qian, Y.-Z. 2006, Phys. Rev. D, 73, 023004
Gaarde, C., et al. 1984, Nucl. Phys. A, 422, 189
Gazit, D., & Bernea, N. 2004, Phys. Rev. C, 70, 048801
Goriely, S., Arnould, M., Borzov, I., & Rayet, M. 2001, A&A, 375, L35
Heger, A., Kolbe, E., Haxton, W. C., Langanke, K., Martínez-Pinedo, G., & Woosley, S. E. 2005, Phys. Lett. B, 606, 258
Keil, M. Th., Raffelt, G. G., & Janka, H.-Th. 2003, ApJ, 590, 971
Kneller, J. P., McLaughlin, G. C., & Brockman, J. 2008, Phys. Rev. D, 77, 045023
Lattimer, J. M., & Prakash, M. 2001, ApJ, 550, 426
Lattimer, J. M., & Yahil, A. 1989, ApJ, 340, 426
Lodders, K., & Amari, S. 2005, Chem. Erde-Geochem., 65, 93
McLean, D. J., Thompsom, M. N., Zumanov, D., McNeill, K. G., Jury, J. W., & Berman, B. L. 1991, Phys. Rev. C, 44, 1137
Millener, D. J., & Kurath, D. 1975, Nucl. Phys. A, 255, 315
Otsuka, T., Suzuki, T., Fujimoto, R., Grawe, H., & Akaishi, Y. 2005, Phys. Rev. Lett., 95, 232502
Pastor, S., & Raffelt, G. 2002, Phys. Rev. Lett., 89, 191101
Primas, F., Duncan, D. K., Peterson, R. C., & Thorburn, J. A. 1999, A&A, 343, 545
Primas, F., Duncan, D. K., & Thorburn, J. A. 1998, ApJ, 506, L51
Pywell, R. E., Berman, B. L., Woodworth, J. G., Jury, J. W., McNeill, K. G., & Thompson, M. N. 1985, Phys. Rev. C, 32, 384
Qian, Y.-Z., & Fuller, G. M. 1995, Phys. Rev. D, 51, 1479
Ramaty, R., Lingenfelter, R. E., & Kozlovsky, B. 2000a, in IAU Symp. 198, The Light Elements and Their Evolution, ed. L. da Silva, M. Spite, & J. R. de Medeiros (Cambridge: Cambridge Univ. Press), 51
Ramaty, R. Scully, S. T., Lingenfelter, R. E., & Kozlovsky, B. 2000b, ApJ, 534, 747
Rauscher, T., Heger, A., Hoffman, R. D., & Woosley, S. E. 2002, ApJ, 576, 323
Rebull, L., Duncan, D., Johansson, S., Thorburn, J., & Fields, B. 1998, ApJ, 507, 387
Shigeyama, T., & Nomoto, K. 1990, ApJ, 360, 242
Shigeyama, T., Nomoto, K., Yamaoka, H., & Thielemann, F.-K. 1992, ApJ, 386, L13
Suzuki, T., Chiba, S., Yoshida, T., Kajino, T., & Otsuka, T. 2006, Phys. Rev. C, 74, 034307
Suzuki, T., Fujimoto, R., & Otsuka, T. 2003a, Phys. Rev. C, 67, 044302
Suzuki, T., Sagawa, H., & Hagino, K. 2003b, Phys. Rev. C, 68, 014317
Takahashi, K., Sato, K., Dalhed, H. E., & Wilson, J. R. 2003, Astropart. Phys., 20, 189
Takahashi, K., Watanabe, M., Sato, K., & Totani, T. 2001, Phys. Rev. D, 64, 093004
Tomàs, R., Kachelrieß, M., Raffelt, G., Dighe, A., Janka, H.-T., & Scheck, L. 2004, J. Cosmol. Astropart. Phys., 9, 15
Warburton, E. K., & Brown, B. A. 1992, Phys. Rev. C, 46, 923
Woosley, S. E., Hartmann, D. H., Hoffman, R. D., & Haxton, W. C. 1990, ApJ, 356, 272
Yamaguchi, A, Terasawa, T, Nakahara, K., & Torizuka, Y. 1971, Phys. Rev. C, 3, 1750
Yoshida, T. 2007, ApJ, 666, 1048
Yoshida, T., Kajino, T., & Hartmann, D. H. 2005a, Phys. Rev. Lett., 94, 231101
Yoshida, T., Kajino, T., Yokomakura, H., Kimura, K, Takamura, A., & Hartmann, D. H. 2006a, Phys. Rev. Lett., 96, 091101
———. 2006b, ApJ, 649, 319
Yoshida, T., Terasawa, M., Kajino, T., & Sumiyoshi, K. 2004, ApJ, 600, 204
Yoshida, T., Umeda, H., & Nomoto, K. 2005b, ApJ, 631, 1039
———. 2008, ApJ, 672, 1043